INVESTIGATION OF INITIAL CONSTRUCTION STAGES OF INCREMENTALLY LAUNCHED POST-TENSIONED CONCRETE BOX BRIDGES

A THESIS SUBMITTED TO
THE GRADUATE SCHOOL OF NATURAL AND APPLIED SCIENCES
OF
MIDDLE EAST TECHNICAL UNIVERSITY

BY

ZAFER ALTINSOY

IN PARTIAL FULFILLMENT OF THE REQUIREMENTS
FOR
THE DEGREE OF MASTER OF SCIENCE
IN
CIVIL ENGINEERING

FEBRUARY 2021

Approval of the thesis:

INVESTIGATION OF INITIAL CONSTRUCTION STAGES OF INCREMENTALLY LAUNCHED POST-TENSIONED CONCRETE BOX BRIDGES

submitted by **ZAFER ALTINSOY** in partial fulfillment of the requirements for the degree of **Master of Science** i**n Civil Engineering, Middle East Technical University** by,

Prof. Dr. Halil Kalıpçılar
Dean, Graduate School of **Natural and Applied Sciences** _____

Prof. Dr. Ahmet Türer
Head of the Department, **Civil Engineering** _____

Prof. Dr. Alp Caner
Supervisor, **Civil Engineering, METU** _____

Examining Committee Members:

Prof. Dr. Ahmet Türer
Civil Engineering, METU _____

Prof. Dr. Alp Caner
Civil Engineering, METU _____

Prof. Dr. Afşin Sarıtaş
Civil Engineering, METU _____

Prof. Dr. Murat Altuğ Erberik
Civil Engineering, METU _____

Assist. Prof. Dr. Kaan Kaatsız
Civil Engineering, Ahi Evran University _____

Date: 12.02.2021

I hereby declare that all information in this document has been obtained and presented in accordance with academic rules and ethical conduct. I also declare that, as required by these rules and conduct, I have fully cited and referenced all material and results that are not original to this work.

Name, Last name : Zafer, Altınsoy

Signature :

ABSTRACT

INVESTIGATION OF INITIAL CONSTRUCTION STAGES OF INCREMENTALLY LAUNCHED POST-TENSIONED CONCRETE BOX BRIDGES

Altınsoy, Zafer
Master of Science, Civil Engineering
Supervisor: Prof. Dr. Alp Caner

February 2021, 111 pages

The incremental launching method is a fast, popular construction method for post-tensioned concrete bridges with mid-span size. It does not require scaffolding under the deck; therefore, it is especially preferred when a bridge passes over a deep valley, high traffic area, or an environmentally sensitive area. Due to its dynamic nature of the launching, the design and optimization of incrementally launching bridges require special attention. A launching nose is used to decrease the moments on the bridge deck during the launch. Infinite beam model and semi-infinite beam models are the most common models for the optimization of the launching noses. Both models are based on advanced stages of the construction; however, to have an accurate design, initial construction stages should also be investigated. In this thesis, a model for the initial construction stages is developed. The new initial stage model includes the movement of the newly casted section and the cantilever deflection of the launching nose, which are not included in the current advanced stage models. The initial stage model is compared with the current advanced stage models. It is observed that moments in the initial stages are higher than the advanced stage moments in some cases. Therefore, the initial stages also should be checked during the design stage.

Effects of launching nose’s design parameters (length, unit weight, and stiffness) on the maximum deflection are investigated. It is found that all three parameters are affecting the maximum deflection, and launching nose length is the most effective parameter.

Keywords: Incremental Launching Method, Launching Nose, Post-tensioned Concrete Bridges, Prestressed Concrete Bridges, Optimization

ÖZ

İTME SÜRME YÖNTEMİYLE YAPILAN ARDGERMELİ KUTU KESİTLİ BETONARME KÖPRÜLERİN İNŞAATLARININ İLK AŞAMALARININ İNCELENMESİ

Altınsoy, Zafer
Yüksek Lisans, İnşaat Mühendisliği
Tez Yöneticisi: Prof. Dr. Alp Caner

Şubat 2021, 111 sayfa

İtme Sürme yöntemi ardgermeli betonarme köprüler için sıklıkla kullanılan hızlı bir yapım yöntemidir. Bu yöntem özellikle köprü derin bir vadiden, yoğun trafikli bir alandan ya da çevresel açıdan hassas bir bölgeden geçerken tercih edilir. İtme Sürmenin dinamik doğasından kaynaklı tasarım ve optimizasyon aşamaları özel dikkat isteyen bir yöntemdir. Yapım sırasında köprü kirişlerinde oluşacak momenti düşürmek için kılavuz gaga kullanılır. Sonsuz kiriş ve yarı-sonsuz kiriş modelleri kılavuz gaga'nın optimizasyon çalışmalarında en çok kullanılan modellerdir. Bu iki model de inşaatın ileri bir aşamada olduğunu varsayıyor ancak doğru bir tasarım için inşaatın ilk aşamaları da dikkate alınmadır. Bu tezde inşaatın ilk aşamaları için yeni bir model geliştirilmiştir. Bu yeni ilk aşamalar modeli hali hazırdaki modellerde olmayan yeni hazırlanan kirişin hareketini ve kılavuz gaganın seğimini de dikkate almaktadır. İlk aşamalar modeliyle ileri aşama modelleri karşılaştırılmıştır. Bu karşılaştırmalarda bazı durumlar için ilk aşamalarda oluşan momentlerin ileri aşamalardan oluşanlardan daha yüksek olduğu gözlemlenmiştir. Bu yüzden tasarım aşamasında ilk aşamaların da kontrolü gereklidir.

Kılavuz gaganın tasarım parametlerinin (boy, birim ağırlık, rijitlik) maksimum seğime etkileri incelenmiştir. En etkilisi kılavuz gaganın boyu olmakla birlikte üç parametrenin de maksimum seğimi etkilediği bulunmuştur.

Anahtar Kelimeler: İtme Sürme Yöntemi, Kılavuz Gaga, Ardgermeli Betonarme Köprüler, Optimizasyon

To my sister, İremnur

ACKNOWLEDGMENTS

I am grateful to my advisor Prof. Dr. Alp Caner, for his guidance and support. His advice helped me with each step of my research. I would also like to thank the members of my thesis committee; Prof. Dr. Ahmet Türer, Prof. Dr. Afşin Sarıtaş, Prof. Dr. Murat Altuğ Erberik, and Assist. Prof. Dr. Kaan Kaatsız for their valuable contributions.

I would like to express my gratitude to all my managers who support me during my master's education: Srijith Chakkadath, Srinivasa Naidu, İrfan Batmaz, and Mustafa Şahin. I also would like to express my gratitude to my teachers who greatly impact my life: Asuman Ant, Ali Orhon, and Asst. Prof. Dr. Onur Pekcan. Thank you for all the advice that you have shared.

I am very grateful to my beloved friends Beril Kumpasoğlu and Hasret Cem Biçer for being with me on my journey in METU for all these years. I will always remember these years as the best of times. I want to thank my dearest friends Ali Mert Şentürk and Dorukhan Özkır, to show me that what a real lifelong friendship means. I also would like to thank to express my gratitude to Hülya Metin and Canan Türkmen. You show me that true friendship is not affected by any distance or border.

I want to thank Tuğba Hato, without her support and encouragement, I would never be able to finish this study. Thank you for believing me even when I did not.

I am very grateful to my mother, Canan Altınsoy and my father, Hicri Altınsoy. Everything I have accomplished is thanks to your support throughout all my life. Finally, I would like to thank my grandmother Kadriye Yaş who passed during my graduate education. You will always be remembered in our hearts.

TABLE OF CONTENTS

LIST OF TABLES

TABLES

LIST OF FIGURES

FIGURES

LIST OF ABBREVIATIONS

ABBREVIATIONS

ILM: Incremental Launching Method

ILB: Incrementally Launched Bridge

FEM: Finite Element Method

ASSHTO: American Association of State Highway and Transportation Official

LIST OF SYMBOLS

SYMBOLS

q: unit weight of the deck

L: span length of the deck

EI: bending stiffness of the deck

q_n: unit weigh of the launching nose

L_n: length of the launching nose

E_nI_n: bending stiffness of the launching nose

x: distance between the tip of the deck and launched support

$\alpha=x/L$

$\alpha_q= q / q_n$: relative unit weight of the launching nose

$\alpha_L= L / L_n$: relative length of the launching nose

$\alpha_{EI}= EI / E_nI_n$: relative bending stiffness of the launching nose

Support A: target support at the start of the launch

Support B: last already launched support at the start of the launch

Support C, D, and E: already launched supports at the start of the launch

J: connection point of nose and bridge deck

S: bending stiffness of the deck

Sn: bending stiffness of the launching nose

Lx: launched Span Length

F_{el}: element force matrix

K_{el}: element stiffness matrix

u: deflection matrix

F_g: global force matrix

K_g: global stiffness matrix

CHAPTER 1

INTRODUCTION

1.1 Aim & Scope

The incremental launching method (ILM) is a relatively new, fast bridge deck construction method that does not require scaffolding under the deck. Therefore, it is mostly preferred when bridges pass over a deep valley, high traffic area, or environmentally sensitive area (Laviolette, Wipf, Lee, Bigelow, & Phares, 2007).

Briefly, in this method, deck segments are prepared behind the abutment and shifted toward to next pier with hydraulic pushers. After the first segment's launching, the second segment prepared on the yard and pushed just like the first one. This process is repeated until the launch of the last segment. During this procedure, all deck cross-sections will undergo cycling positive and negative bending moments rather than service life situation where positive moment affects the deck sections, and negative moments affects the support sections. Also, the front section will act as a cantilever before it reaches the next support; this will create tremendously high negative moments on the last support section. Therefore, ILM requires special techniques to control these cycling moments and the cantilever moment.

Lightweight steel launching noses attached to the front deck are used to reduce these moments. This nose will increase the total cost of the construction. Engineers aim to optimize the launching nose design to reduce the construction cost. The dynamic nature of launching and interaction of launching nose and deck makes the analysis of the bridge more complicated than the ordinary bridges; therefore, different methods are developed to optimize the design of the launching nose. These methods

focused on the advanced stages of the launching. However, the initial stages of the construction also should be checked.

This thesis aims to prepare a simple model of the initial construction stages of incrementally launched bridges for the preliminary optimization of the launching nose. This new initial stage model also considers the movement of the newly casted section at the yard and deflection of the cantilever launching nose, which were not considered in the current advanced stage models.

Chapter 2 Literature Review starts with the history and current research topics on the incremental launching method. Then details of the incremental launching method with its advantages and disadvantages are explained.

In Chapter 3, the advanced stage analysis model and optimization methods are explained. Current preliminary design models for the optimization studies are the infinite beam model and the semi-infinite beam model. These advanced stage models are explained in detail. Then current optimization studies: trial and error method, analytical method, and numerical method are explained.

The semi-infinite beam model is an advanced construction stage model that aims to represent the infinite beam model's behavior with a defined number of spans. An analysis code for the semi-infinite beam model is developed in MATLAB; then, this code is used for its comparison against the infinite beam model.

Chapter 4 explains the new initial stage analysis model. Analysis code for the new initial stage model is also developed in MATLAB. Details of the code and the method are explained. Then, the initial stage model is compared with the advanced stage models.

This new method also includes the deflection control. Current methods are focused on bending moments on the spans, and they do not take deflection into account, but large deflections occur on the cantilever launching nose during the launch. Therefore, launching nose design parameters' effects on tip deflection are examined. Deflections are examined on both theoretical and realistic models.

MATLAB code prepared for the initial construction stage analysis is shared in Appendix A. This analysis code's verification with the SAP2000 structural analysis software is explained in Appendix B.

Post-tensioned reinforced concrete bridges are chosen for this thesis due to their popularity with this method, but most of the equations are also applicable for the other types of bridges (steel, composite, etc.).

CHAPTER 2

LITERATURE REVIEW

2.1 History & Current Status

Figure 2.1. Launch of the Rio Caroni Bridge (Rosignoli, 2014)

The incremental launching method (ILM) first started to be used in steel bridges constructions in the late 19th century (Fontan, Diaz, Baldomir, & Hernandez, 2010); however, the first one is unknown. Its adaptation on concrete bridges and studies on the topic started in the mid-20th century. The first incremental launched concrete bridge without falsework is constructed on the Caroni River in Venezuela (Zellner & Svensson, 1983) in 1961, designed by Fritz Leonhardt. 480m post-tensioned concrete deck and 17m steel launching nose for deflection control are launched as

one unit (Figure 2.1). In the current practice, the launching nose method is still in use, but bridges are not launched as a whole. They launched as one segment (approximately equal to half a span length) at a time, which decreases the area requirement behind the abutment. The first example of this method is applied on a bridge on Inn River (Austria) in 1968 (Zellner & Svensson, 1983).

It is estimated ILM is used in more than 1000 bridges all around the world (Laviolette et al., 2007). The exact number of the incrementally launched bridges in Turkey is unknown, but the Kobuk and Bayındır Bridges in Ankara (Popov & Seliverstov, 1998), Çayırköy Viaduct in Kocaeli (Özel, Kutsal, & Özkul, 2019) are some examples in Turkey.

ILM does not require scaffolding under the deck. Therefore, it is generally used when a bridge passed a deep valley, environmentally sensitive area, or high traffic area. The bridge deck will be constructed on these areas without affecting the area under the deck. Common span lengths of post-tensioned concrete ILBs are 40m to 65m (Rosignoli, 2000). It can also be applied on bridges with span lengths longer than 70m, but they generally require temporary piers between main piers (Marchetti, 1984). These span sizes are changes for the different types of bridges. For example, Vaux Viaduct is a steel-concrete composite bridge with a maximum span length of 130m and constructed without temporary piers (Navarro, Lebet, & Beylounü, 2000).

Research on ILM is increasing each day, which focuses on different aspects of the method: analysis, optimization, case studies, and material behaviors. Several textbooks are written on the area: *Incrementally Launched Bridges: Design and Construction* is written by Göhler & Pearson (2000) and *Bridge Launching* by Rosignoli (2002, 2014). AASHTO published a comprehensive report on the topic: *Bridge Construction Practices Using Incremental Launching* (Laviolette et al., 2007).

Due to the dynamic nature of ILM, the usage of traditional commercial analysis software is not always sufficient. For each launching phase, different configuration needs to be analyzed with the chosen increment step size. Studies offer different and

faster solution methods for incrementally launched bridges. Rosignoli (1997) suggests using the reduced transfer matrix (RTM) based on the transfer matrix method. Sasmal et al. (2004) developed a computer software based on the transfer matrix method for the analysis of ILB, which also taken account settlement and thermal effects. Sasmal & Ramanjaneyulu (2006) proposed the transient transfer matrix (TTM) method, which also considers the effects of prestressing, linearly varies weighted launching nose, and support bearing stiffness. Arici & Granata (2007) further improved the method to apply on curved bridges, which also considers torsional effects, and Granata (2014) analyzed non-uniform torsion on ILBs. Shojaei et al. (2015) mentioned these two methods are insufficient for parametric studies. Also, they are not commonly used methods in optimization studies. Therefore, RTM and TTM are out of this thesis's scope.

Apart from TTM and RTM, Marchetti (1984) developed a simple nose-deck model. Rosignoli (1998) further developed this nose-deck interaction model with the assumption of the infinite section behind the launching span. This model is mostly the standard model the optimization studies.

Later Shojaei et al. (2015) developed a simplified semi-infinite beam model based on their finite element modeling. Also, Xu & Shao (2012) suggested an advanced new beam element for finite element solutions of ILBs. These infinite and semi-infinite beam models' limitations and comparisons are discussed in detail in Chapter 3.

Advancements in design studies lead to different and more accurate optimization studies. Rosignoli (1998) suggested keeping negative moments on the last support at the minimum using trial and error to have the optimum launching nose. Wang et al. (2010) also followed a similar approach and developed a relationship between optimum relative unit weight and length. Rather than using trial and error or analytical equations, the feasible directions optimization algorithm is also used to have an optimized launching nose (Fontan et al., 2010; Hirmand, Moghadam, & Riahi, 2013). Later, Fontán et al. (2013) and Hernandez & Fontan (2014) further

developed the method to optimize cross-section and launching nose simultaneously. Details of the optimization methods are explained in Chapter 3.2.

During the launch, steel launching noses are subjected to concentrated forces from the bridge supports, which travel through the length. Launching noses of the post-tensioned concrete box bridges are mostly consist of two I-beams with slender web sections. Due to this slender shape, patch loading problems might occur on the launching nose. This phenomenon is studied extensively. Granath (1998) conducted a laboratory experiment to investigate the distribution of support reactions on the steel girder. Granath et al. (2000) also made numerical analyses studies on the patch loading phenomenon. Finally, Granath (2000) suggested a serviceability limit states for I-shaped steel girders subjected to patch loading. Chacón & Zorrilla (2015) proposed a strain gauge arrangement as a structural health monitoring method to investigate patch loading phenomena during the launch. Chacón et al. (2016) did an experiment for the numerical validation of the incremental launching method of a steel bridge.

Due to different loads on the construction phase and service phase, prestressing schemes of prestressed concrete bridges require special attention and studied by different researchers (Granata, 2015; Rosignoli, 1999). Apart from post-tensioned concrete bridges, the incremental launching method is also used and studied on different types of bridges. Wu et al. (2018) studied the effects of height difference between a steel bridge's trusses during the launching. Hu et al. (2015) conducted laboratory testing on a hybrid arc-girder bridge.

If the required preventative actions were not taken, problems might occur during the construction of the ILBs. Figure 2.2 shows the collapse of the San Cristobal Bridge in Mexico (Nader, Manzanarez, Lopez-Jara, & De La Mora, 2007). In the bridge, shear studs between the steel girder and concrete deck failed due to their insufficient numbers. This failure causes the loss of composite action and consequently the failure of the bridge.

Figure 2.2. Collapse of the San Cristobal Bridge (Nader et al., 2007)

Several notable examples of the recent incremental bridges are Reno Bridge in Italy (Ferretti, 2016; Furlanetto, Torricelli, & Marchiondelli, 2010), Millau Viaduct in France (Buonomo et al., 2004), Ile Falcon Bridge (Favre, Badoux, Burdet, & Laurencet, 1999), and Vaux Viaduct in Switzerland (Navarro et al., 2000), Panval Nadhi Viaduct in India (Ramakrishna & Sankaralingam, 1997), M7 motorway viaducts in Hungary (Lontai, Nagy, & Mihalek, 2008), Woronora Bridge in Australia (Bennett & Taylor, 2002), River Esk Bridge (Liddle, 2010), Stewarts River and the Camden Haven River Bridge in the UK (Burkitt, Team, Structures, & Alliance, 2009).

Other than the classic post-tensioned concrete box girder bridges, other types of bridges were also constructed with ILM. One example is Ilsun Bridge in South Korea, the world's longest and widest prestressed concrete box girder with a corrugated steel web section bridge (Jung, Kim, Sim, & Kim, 2011). Another example is Jiubao Bridge in Hangzhou, China; it is a hybrid arch-girder bridge constructed using ILM (Hu et al., 2015; Shao, 2013). Table 2.1 shows the notable

examples of the incremental launching bridges with their length, maximum span length, and launching nose length.

Table 2.1 Examples of the Incrementally Launched Bridges

Title	Year	Location	Type	Max Span Length	Total Length	Nose Length
Mechelse Steenweg	2001	Belgium	Post-Tensioned T-Section Concrete Box	17	128	10
Camden Haven	2009	Australia	Post-Tensioned Concrete Box	29	174	15
Stewards Bridge	2009	Australia	Post-Tensioned Concrete Box	38	274	28
Panval Nadhi	1994	India	Post-Tensioned Concrete Box	40	424	30
River Esk Bridge	2008	England	Steel-Concrete Composite	52	180	15
Ile Falcon Bridge	1998	Switzerland	Post-Tensioned Concrete Box	73	720	26
Reno Bridge	2006	Italy	Post-Tensioned Concrete Box	93	528	32
The Stoney	1997	Canada	Post-Tensioned Concrete Box	102	476	32
Vaux Viaduct	1999	Switzerland	Steel-Concrete Composite	130	945	35
San Cristobal	2006	Mexico	Steel-Concrete Composite	180	323	NA

2.2 Application

In the incremental launching method, deck segments are prepared behind the abutment. These segments are generally cast around half a span length (20-30m) (Rosignoli, 1998). After the casting, it pushed (launched) up to the next support pier, and the same process repeated for all decks. For shorter bridges, pistons connected to the backside of the deck are commonly used for pushing. For longer bridges, friction launchers (Figure 2.3) connected to under the deck are used (Rosignoli, 2000).

Figure 2.3. Friction Launchers (Furlanetto et al., 2010)

Low friction Neoflon (PTFE) pads are used at the top of the bearings on the intermediate piers to reduce the friction between the concrete deck and the piers. The kinetic friction coefficient of well-lubricated Neoflon pads is lower than 2% (Rosignoli, 2014). This low friction will decrease the required launching forces. It will also mitigate the extra bending moments that occur on the deck due to friction.

Lateral guides are used to align deck direction during the launching to ensure it stays in the intended direction. These lateral guides also resist the transverse forces acting

on the girders, such as wind and seismic effects during the launching. Therefore, transverse wind forces and earthquake effects should also be considered in lateral guides' design (Rosignoli, 2014).

The most common type of section of ILB is box sections, which have high torsion rigidity. The deck girder should also be straight or have a constant curvature so that each segment of the bridge will follow the same path over the piers, from start to end. Figure 2.4 and Figure 2.5 show a picture and drawing of an incrementally launched bridge with constant curvature.

Figure 2.4. Curved Mechelse Steenweg Bridge (De Clercq & De Ridder, 2003)

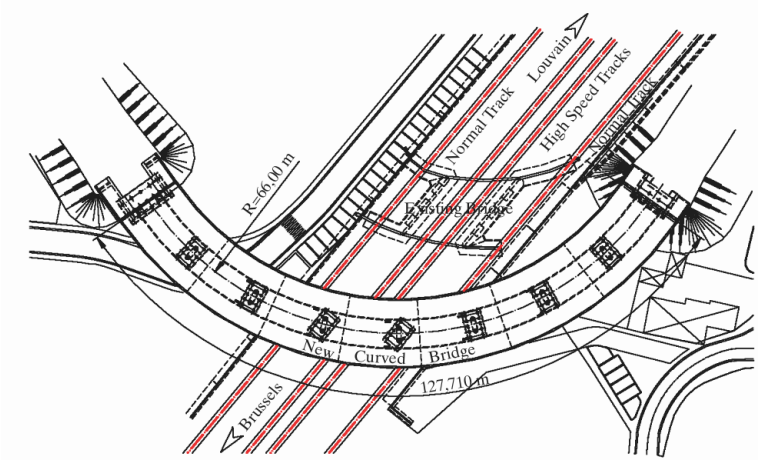

Figure 2.5. Curved Mechelse Steenweg Bridge drawing (De Clercq & De Ridder, 2003)

While the basic principle of the method is relatively simple, its implementation requires special attention. Due to the nature of the ILM, the following issues occur during the bridge's construction, and they need to be checked and solved prior to the construction. Firstly, when the first segment is pushed, it will act as a cantilever beam, and its open end will deflect due to its own self-weight. This vertical deflection will increase up until the span reaches the next pier. When the tip is reached the next pier, it will be hoisted with hydraulic equipment. This vertical deflection should be less than a defined maximum value so that it can be easily realigned.

Finally, on a fully constructed bridge, the support sections are undergoing negative bending moments, and span sections are undergoing positive bending moments. However, it is not the case for the construction phase of incrementally launched bridges. During construction, each cross-section of the bridge deck will act as both the mid-span section and supports section alternately, as shown in Figure 2.6. Therefore, all cross-sections will be under the cycling loading of both positive and negative bending moments. Due to this situation, similar cross-sections are used on both midspan and support sections, unlike the bridges built with other methods.

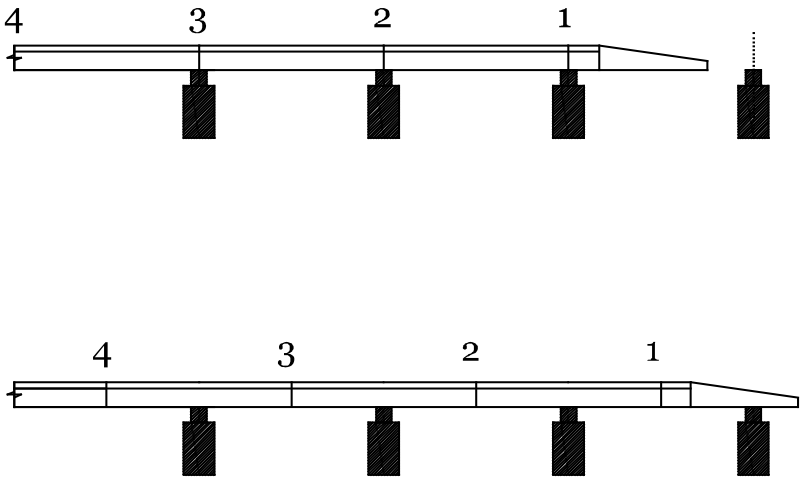

Figure 2.6. Configuration changes during the launch

Different active and passive solutions are made to limit these problems. One solution is using a cable-stayed system (Figure 2.7), which consists of one vertical mast and tendons connecting the tip of the bridge and two spans behind (Rosignoli, 2002). When the frontier section passes the support and becomes a cantilever, stresses on tendons increased with prestressing equipment. This new tension force on the deck will decrease the vertical deflection and carry the span's self-weight, which causes a decrease of the excessive moment. However, this technique is discouraged due to the requirement of continuous adjustments of the cable forces, complexity, and potential of creating stress concentration (Rosignoli, 1998). Thus, this method is beyond this thesis's scope.

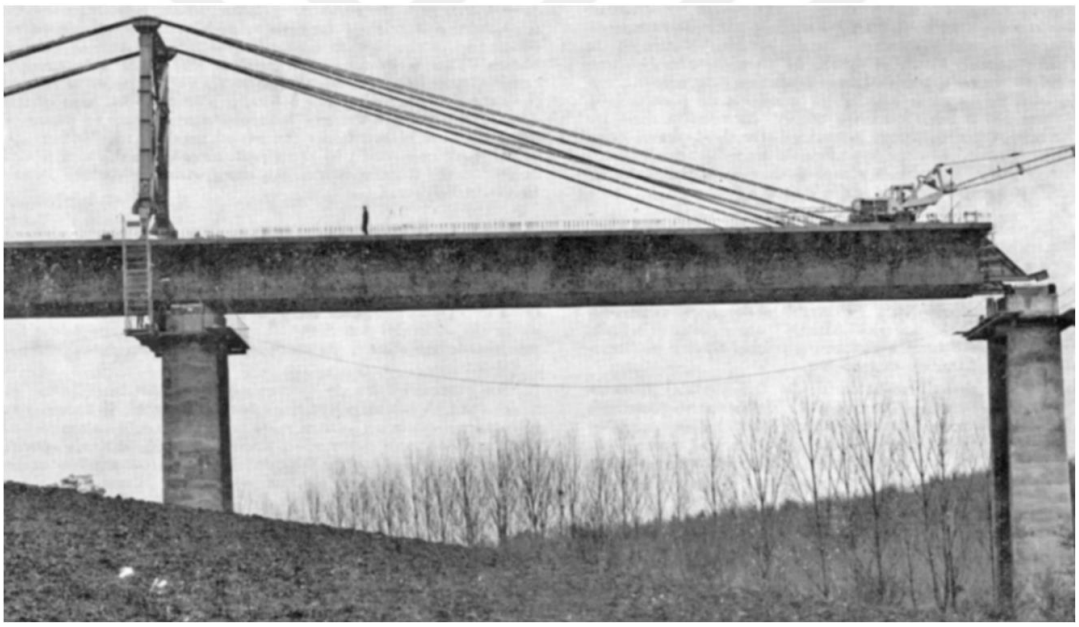

Figure 2.7. Bridge Launching with Cable-Stayed System (Rosignoli, 2014)

The deflection of the cantilever part increases with the span size. Longer spans cause longer cantilever sections, which cause higher deflection and bending moment values. As a solution, temporary piers (Figure 2.8) are used to decrease the span lengths. These piers are constructed on the mid-length of the spans prior to the launching, and they halved the span length. After the construction of the bridge, they

dismantled. This method is time-consuming and increases the material cost. Therefore, it is only optimum for the bridge with longer spans.

Figure 2.8. Millau Viaduct before the last launch (Buonomo et al., 2004)

The main cause of the deflection and excessive moments is the self-weight of the cantilever section, so the solution is apparently lightening the self-weight. The most common solution to this problem is using a launching nose to decrease the weight. Launching nose is a steel girder that is much lighter than the original concrete deck. Thanks to its lightweight, both deflection and moment due to cantilever action will decrease.

Launching noses varies in shapes and sizes according to the requirement of the project. The most common type for steel bridges is truss sections (Figure 2.9). And two tapered I-girder on two sides, braced with each other (Figure 2.10) is the standard geometry for post-tensioned concrete bridges (Rosignoli, 2002). The tip of the launching nose will be subjected to lower forces and moments than the nose's starting part. Therefore, it allows the usage of tapered girders. This tapered geometry will reduce the nose weight and the cost.

Figure 2.9. Steel launching nose with truss system (Rosignoli, 2014)

Figure 2.10. Steel launching nose with I-girders (Lopez, 2010)

Even though the launching nose decreases the vertical deflection and bending moment, each cross-section still undergoes both positive and negative moments alternatively. Bridge cross-sections should be designed according to these moments, and the launching nose should be designed to minimize these moments.

2.3 Advantages & Disadvantages

The incremental launching method has the following advantages over the more traditional methods:

- Falsework, which is a costly and time-consuming activity, is not required under the deck.
- ILM has a lower impact on the area under the bridge due to the non-requirement of the falsework. Especially preferable for bridges pass over a deep valley, high traffic, or environmentally sensitive area.
- ILM does not require crane transportation (for precast girders) or concrete pumps (for cast-in-situ) under the deck as the balanced cantilever method requires.
- Girder segments can be prepared longer than the balanced cantilever bridges, which cause a lesser number of connection joints and potential weak points (Rosignoli, 1998).
- Preparation of the girder segments on the ground increases work safety.
- The concentrated working area increases the overall quality. Work can be monitored easily, and the process can be automized.

And the following disadvantages:

- ILM needs specials equipment (launching nose, temporary bearings, and hydraulic jacks), which increases the cost.
- While the method is widely accepted as economical up to 65m span lengths, for longer spans, construction of the temporary piers is required, which increases the overall construction cost.

- During the launching phase, the bridge deck and supports will be under different loading conditions than the final stage. Therefore, it should be designed with special considerations to resist both final and launching phase forces, which may increase the deck dimensions and cost.

CHAPTER 3

ADVANCED STAGE ANALYSIS AND OPTIMIZATION METHODS

3.1 Launching Nose – Deck Interaction Analysis

An incrementally launched bridge will undergo completely different forces and moments during the construction stage. Calculation of these forces requires special attention. Each launching session consists of two phases. Phase 1 ($0 \leq x < L - L_n$) (Figure 3.1) is started with the pushing of the newly casted section and continues up to the tip of the launching nose reach the target pier, and Phase 2 ($L - L_n \leq x <$ L) (Figure 3.7) began when the launching nose reaches the target pier and ends when the concrete deck reaches the target pier. Deck behavior changes dramatically between these phases due to the addition of support A to the system; therefore, they require different force and moment equations.

Different models exist to understand the behavior of these stages. They explain the moments, shear forces, and rotations on the support points and spans. Most of the studies use the same dimensionless theoretical model, which helps us to understand the behavior with a generalized example. This theoretical model is based on three main parameters: relative length (α_L), relative unit weight (α_q), and relative bending stiffness (α_{EI}) of the launching nose to the bridge deck. It can also apply to real models with some small modifications. The most commonly used models for the optimization studies are the infinite beam model and semi-infinite beam model; both are explained in this chapter. The following notation will be used:

- q: unit weight of the deck
- L: span length of the deck
- EI: bending stiffness of the deck
- q_n: unit weigh of the launching nose

- L_n: length of the launching nose
- E_nI_n: bending stiffness of the launching nose
- x: distance between the tip of the deck and launched support
- $\alpha=x/L$
- $\alpha_q= q / q_n$: relative unit weight of the launching nose
- $\alpha_L= L / L_n$: relative length of the launching nose
- $\alpha_{EI}= EI / E_nI_n$: relative bending stiffness of the launching nose
- Support A: target support at the start of the launch
- Support B: last already launched support at the start of the launch
- Support C, D, and E: already launched supports at the start of the launch

3.1.1 Infinite Beam Model

The infinite beam model is a commonly used model for ILB developed by Rosignoli (1998). This model has the following assumptions:

- Both nose and deck have constant stiffness and unit weight.
- The bridge consist of many same lengths spans behind the support C. Therefore, the system is assumed to be a continuous beam with infinite spans.
- Launch prestressing is centroidal, so it will not create any additional unknown redundant.

Regarding these assumptions:

- It is common to bridge decks to have constant cross-sections but, launching noses are generally consist of tapered steel girders or truss sections. They vary in both stiffness and weight from one end to the other. However, Shojaei et al. (2015) mention that it only causes a small error (<2%). So, this assumption is applicable.
- Same length spans are possible, but the following calculations are only applicable for advanced construction steps where lots of sections are already

launched. For the initial construction stages, different models are required. Therefore, a new initial stage model is developed and discussed in Chapter 4: Initial Stage Analysis Model.

3.1.1.1 Phase 1: $0 \leq x < L - L_n$

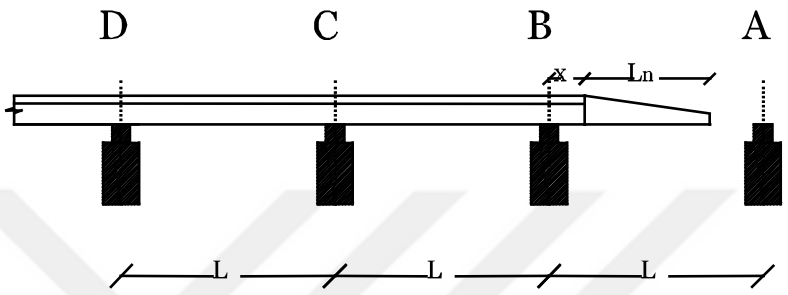

Figure 3.1. Phase 1 of the Launching

Figure 3.1 shows the configuration of the bridge during phase 1. A continuous beam system under its own dead load with pin supports only creates moments on intermediate supports; therefore, at the start of the launch, already launched sections at the behind of support B are not effective on the moment on support B. Moment of support B (M_{B1}) is only related to the cantilever launching nose's weight and length. Therefore M_{B1} moment is (Rosignoli, 1998):

$$\frac{M_{B1}}{qL^2} = -\frac{q_n}{2q}\left(\frac{L_n}{L}\right)^2 \tag{3.1}$$

When launching started concrete deck also became cantilever and increase the negative moment on support B:

$$M_{B1} = -\frac{q * x^2}{2} - L_n q_n (x + \frac{L_n}{2}) \tag{3.2}$$

And its dimensionless presentation:

$$\frac{M_{B1}}{qL^2} = -\frac{\alpha^2}{2} - \alpha_L \alpha_q (\alpha + \frac{\alpha_L}{2}) \tag{3.3}$$

Figure 3.2 shows the bending moment on support B during the launch for chosen parameters (L_n=0.5, q_n=0.1). The x axis shows the distance between the tip of the launched concrete deck and the last support (α) of the theoretical model. the y axis shows the dimensionless form of the bending moment at support B (M/ql^2). -1/12 ($1/ql^2$) is the typical moment value for support joints on a continuous beam with many equal spans under its own dead weights (Fontan et al., 2010). Therefore, it is also shown in the figures. The negative bending moment on support B increases continuously from the start of the launch to the end of phase 1.

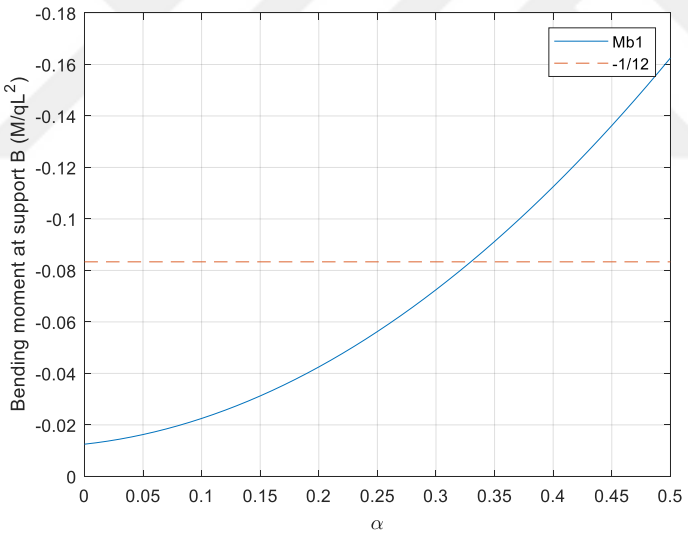

Figure 3.2. Bending Moment at Support B during phase 1 (α_L =0.5 α_q =0.1)

M_C equation is as follows (Rosignoli, 1998):

$$\frac{M_C}{qL^2} = -\frac{C_5 + C_4}{C_3 + C}\frac{1}{qL^2} - \frac{C_2}{C_3 + C_1}\frac{M_{B1}}{qL^2} \tag{3.4}$$

With the following constants:

$$C_1 = \frac{1}{3EI} \tag{3.5}$$

$$C_2 = \frac{1}{6EI} \tag{3.6}$$

$$C_3 = \frac{1}{2\sqrt{3}EI} \tag{3.7}$$

$$C_4 = \frac{qL^3}{24EI} \tag{3.8}$$

$$C_5 = \frac{qL^3}{24\ \sqrt{3}EI} \tag{3.9}$$

If we put constants in the equation, it becomes:

$$\frac{M_C}{qL^2} = -\frac{1+\sqrt{3}}{4\left(3+2\sqrt{3}\right)} - \frac{\sqrt{3}}{3+2\sqrt{3}}\frac{M_{B1}}{qL^2} \tag{3.10}$$

Figure 3.3 shows the negative bending moment on support C during phase 1 of the launch for chosen parameters (α_L =0.5 α_q =0.1). Contrary to M_B, M_C starts with the maximum value and decreases until the end of phase 1.

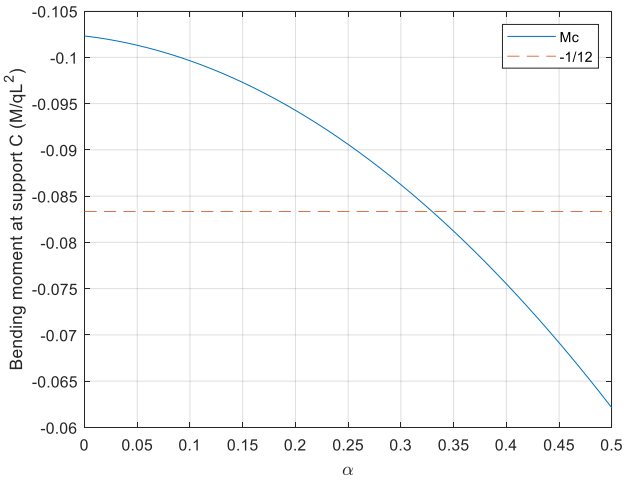

Figure 3.3. Bending Moment at Support C During Phase 1 (α_L =0.5 α_q =0.1)

Shear on support B (R_B) is as below (Rosignoli, 1998):

$$\frac{R_B}{qL} = \frac{M_c}{qL^2} + \frac{(1+\alpha)^2}{2} + \frac{q_n}{q}\frac{L_n}{L}\left(1 + \alpha + \frac{L_n}{2L}\right) \tag{3.11}$$

And if we include M_{B1} in R_B equation, it becomes (3.12):

$$\frac{R_B}{qL} = \frac{M_C}{qL^2} - \frac{M_{B1}}{qL^2} + (\frac{1}{2} + \alpha + \alpha_q + q_L) \tag{3.12}$$

$$R_B = \frac{M_c}{L} - \frac{M_{B1}}{L} + (\frac{qL}{2} + xq + q_n L_n) \tag{3.13}$$

Figure 3.4 shows the shear force change on support B during phase 1 for the chosen parameters (α_L =0.5 α_q =0.1)

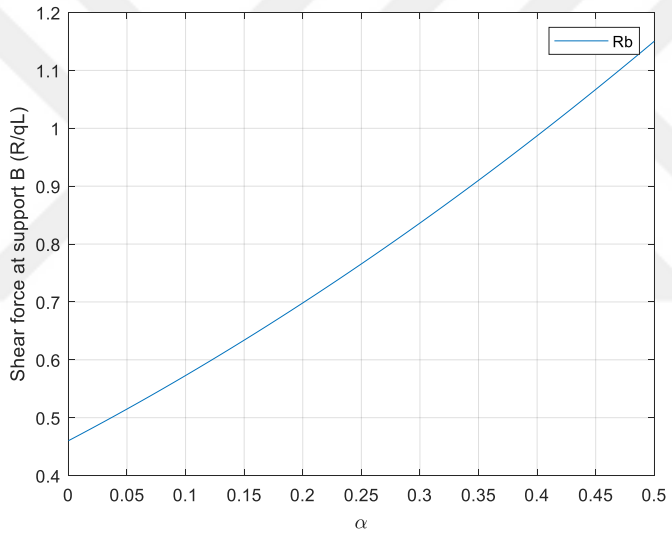

Figure 3.4. Shear Force at Support B during Phase 1 (α_L =0.5 α_q =0.1)

In most cases, the maximum negative moment condition occurs on support B rather than support C or other rear supports. Therefore, most of the studies focus on the maximum moment on support B and parameters that affect it. Figure 3.5 and Figure 3.6 show the effects of the launching nose length and unit weight on the support moment. The graph for stiffness change is not shown because it is not an effective parameter in phase 1 moments.

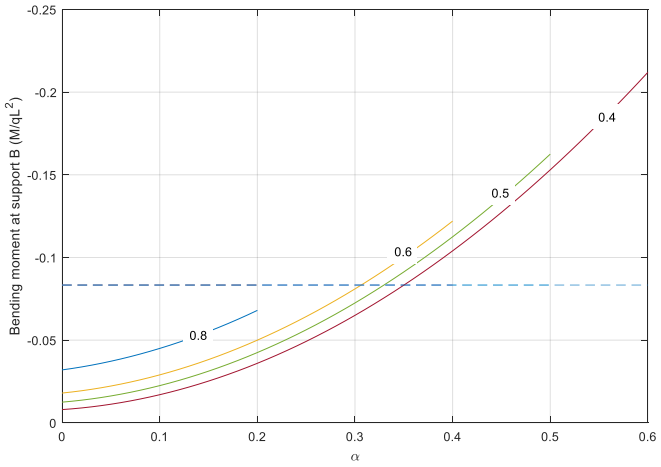

Figure 3.5. Bending Moment at Support B during phase 1 for different relative nose lengths (α_q =0.1)

Figure 3.5 shows the relation between bending moment and relative launching nose length. A shorter launching nose causes lower bending moments on support B than the longer launching nose for a chosen intermediate point. However, it is not correct for the peak moment values. Shorter noses cause higher peak moment values than the longer launching noses on phase 1.

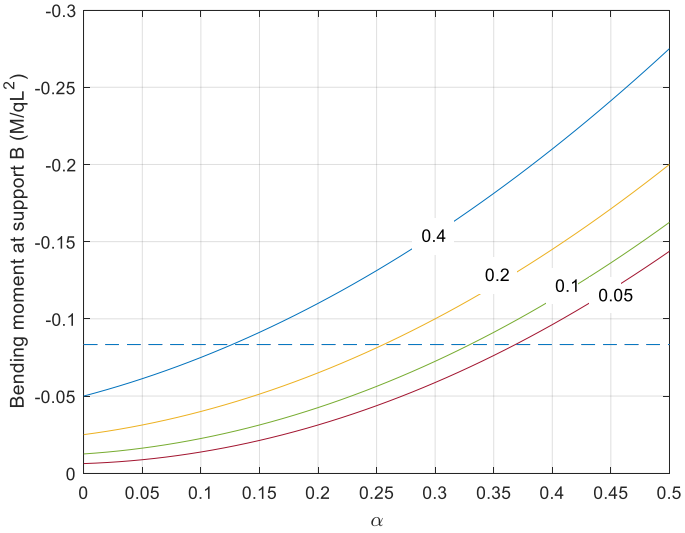

Figure 3.6. Bending Moment at Support B during phase 1 for different relative unit weights (α_L =0.5)

Figure 3.6 shows bending moment changes with respect to launching nose relative unit weights. Heavier noses cause higher moments than lighter noses.

From the formulations and graphs above, we can conclude that the relative launching nose unit weight and unit length are important parameters to determine the moment of support B. At the same time, stiffness is not effective in phase 1. It is also found that longer and lighter launching noses cause lower bending moments on support B during phase 1.

3.1.1.2 Phase 2: $L - L_n \leq x < 1$

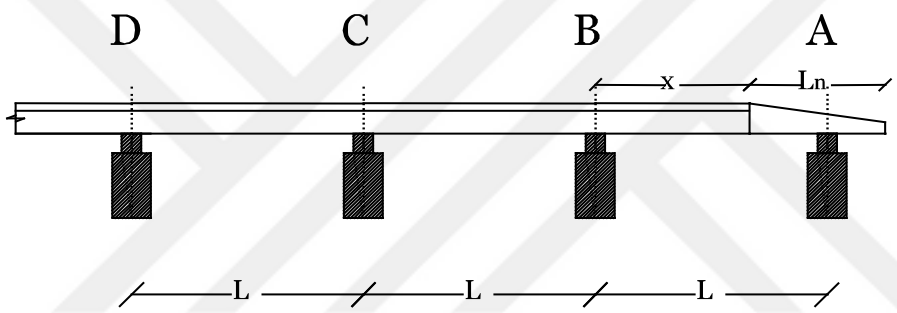

Figure 3.7. Phase 2 of the Launching

Phase 2 (Figure 3.7) starts when the launching nose reached the bearings on target support A. When the tip of the launching nose reaches the support A, it may not be on the same level with temporary bearings due to vertical deflection. In that case, it hoisted with special equipment to realign with a temporary bearing on support A. In Phase 1, the launching deck was cantilever; however, when it reaches support A, the dead load of the launching section will be carried by both support A and B, which will reduce the negative bending moment on support B. Due to different configuration and the addition of support A, the bending moment formula for support B is changed, and stiffness also became a part of the equation (Rosignoli, 1998):

$$\frac{M_{B2}}{qL^2} = \frac{\left(\frac{C_5 + C_4}{C_3 + C_1} C_2 - C_4 - C_8\right) \frac{1}{qL^2} + \frac{1}{2} \frac{q_n}{q} C_7 \left(\frac{L_n}{L} + \alpha - 1\right)^2}{C_1 + C_6 - \frac{C_2^2}{C_3 + C_1}} \tag{3.14}$$

With the following new constants (Rosignoli, 1998):

$$C_6 = \frac{1}{3EI} \left[1 + \left(\frac{EI}{E_n I_n} - 1\right)(1 - \alpha)^3\right] \tag{3.15}$$

$$C_7 = \frac{1}{EI}\left[\alpha^2 \left(\frac{1}{2} - \frac{\alpha}{3}\right) + \frac{EI}{E_n I_n}\left(\frac{1}{6} - \frac{\alpha^2}{2} + \frac{\alpha^3}{3}\right)\right] \tag{3.16}$$

$$\begin{aligned} C_8 = {} & \frac{qL^3}{2EI}\left\{\left[\alpha(2 - \alpha) + \frac{q_n}{q}(1 - \alpha)^2\right]\left(\frac{\alpha^2}{2} - \frac{\alpha^3}{3}\right) - \left(\frac{\alpha^3}{3} - \frac{\alpha^4}{4}\right)\right\} \\ & + \frac{qL^3}{24EI}\frac{EI}{E_n I_n}\left[4\alpha^2(1 - \alpha)^3 + \frac{q_n}{q}(4\alpha^5 - 15\alpha^4 + 20\alpha^3 - 10\alpha^2 + 1)\right] \end{aligned} \tag{3.17}$$

Figure 3.8 shows the bending moment changes on support B during phase 1 and 2. M_B reduces drastically when the launching nose reaches the next support A. At the start of phase 2, the previously cantilever launching nose and the bridge deck started to be carried by both A and B supports. During phase 2, the launching nose again became a cantilever, and it causes an increase at the moment on both supports.

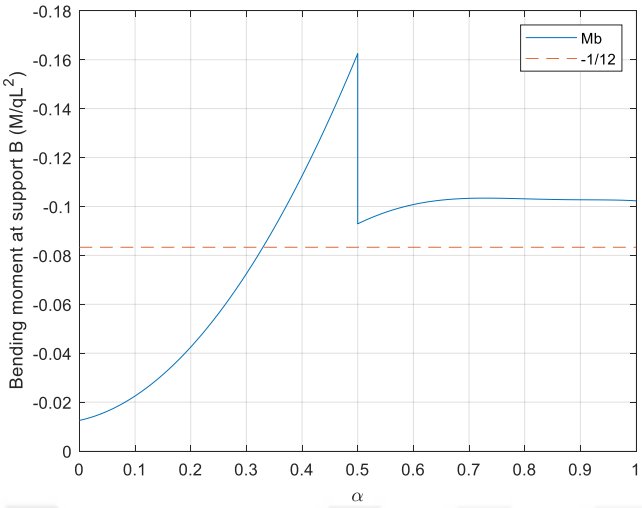

Figure 3.8. Bending Moment at Support B during launch (α_L =0.5 α_q =0.1 α_{EI} =0.2)

The phase 2 M_C equation is the same as phase 1. M_C changes over the launching are shown in Figure 3.9. M_C is like the opposite of the M_B; it increases at phase change and then slowly decreases up to the end of the launch.

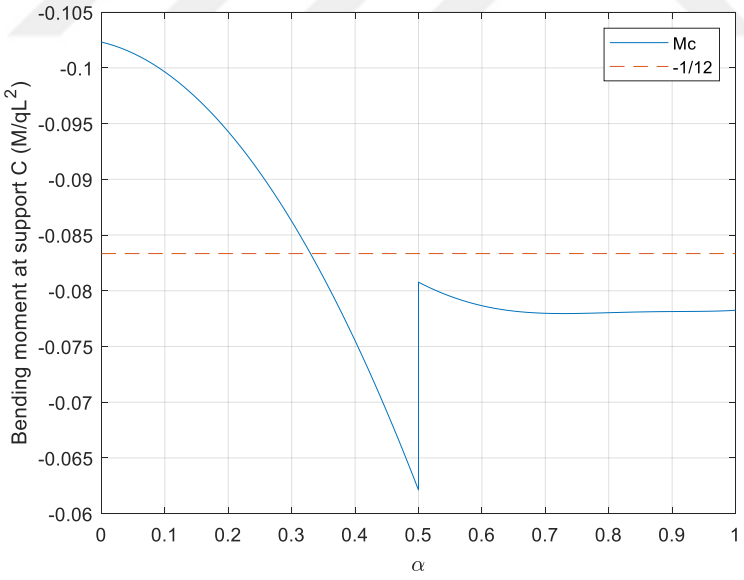

Figure 3.9. Bending Moment at Support C during launch (α_L =0.5 α_q =0.1 α_{EI} =0.2)

When the launching nose reaches support A at the start of phase 2, it started to be carried by support A, and it causes a reaction on support A. Equation of shear force at support A (R_a) is (Rosignoli, 1998):

$$\frac{R_A}{qL} = \frac{M_{B2}}{qL^2} + \frac{\alpha^2}{2} + \frac{q_n}{q}\frac{L_n}{L}\left(\alpha + \frac{L_n}{2L}\right) \tag{3.18}$$

The above equation (3.18) can also be written as follows (3.19). M_{B1} is the moment formula due to the cantilever action from phase 1. Figure 3.10 shows R_a change during phase 2. It continues to increase up to the end of the launch.

$$\frac{R_A}{qL} = \frac{M_{B2}}{qL^2} - \frac{M_{B1}}{qL^2} \tag{3.19}$$

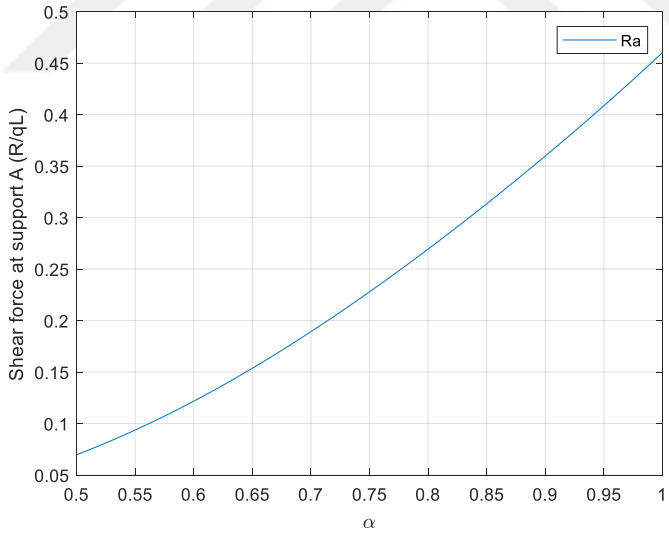

Figure 3.10. Shear Force at Support A during phase 2 (α_L =0.5 α_q =0.1 α_{EI} =0.2)

Maximum span moment equations on span AB (3.20) and BC (3.21) are shown below (Rosignoli, 1998). Figure 3.11 shows that the maximum moment on the front span gradually increases up to the end of the launch. Figure 3.12 shows the maximum

moment on the BC span during the launch. 1/24 ($1/ql^2$) is a typical maximum moment value for continuous beam spans; therefore, it is also shown for reference.

$$\frac{M_{AB,max}}{qL^2} = \frac{R_A}{qL}\left(1 - \alpha - \frac{q_n}{q}\frac{L_n}{L}\right) + \frac{1}{2}\left(\frac{R_A}{qL}\right)^2 + \frac{1}{2}\frac{q_n}{q}\left(\frac{Ln}{L}\right)^2\left(\frac{q_n}{q} - 1\right) \quad (3.20)$$

$$\frac{M_{BC,max}}{qL^2} = \frac{1}{2}\left(\frac{M_C}{qL^2} - \frac{M_B}{qL^2} + \frac{1}{2}\right)^2 + \frac{M_B}{qL^2} \quad (3.21)$$

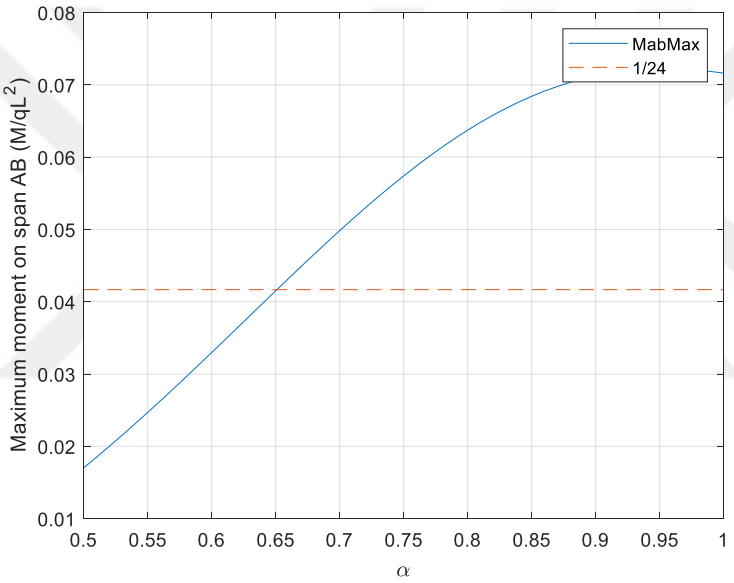

Figure 3.11. Maximum Moment on Span AB during phase 2 (α_L =0.5 α_q =0.1 α_{EI} =0.2)

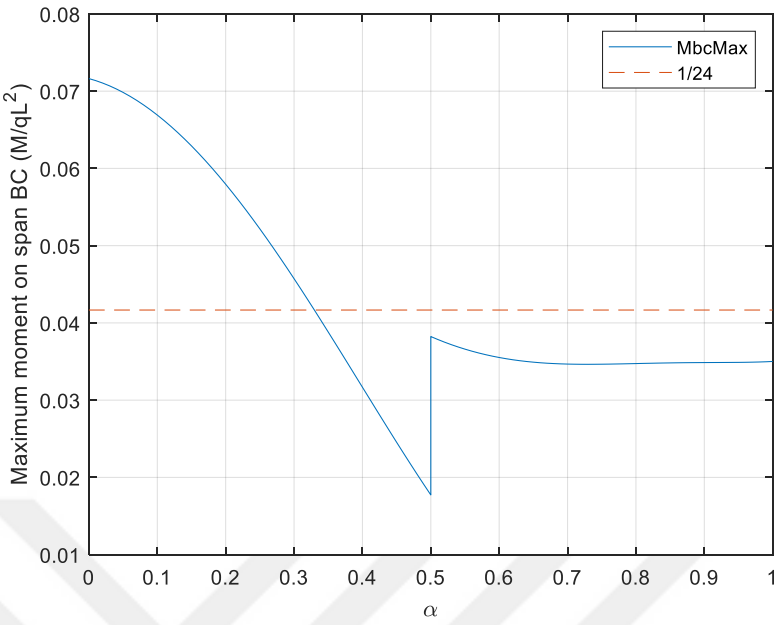

Figure 3.12. Maximum Moment on Span BC during launch (α_L =0.5 α_q =0.1 α_{EI} =0.2)

The bending moment at the nose-deck interface formula during the launch is equation (3.22). Figure 3.13 shows the change of this moment during the launch. In phase 1, the moment on connection is only due to the self-weight of the launching nose. Therefore, it is constant and negative up to the end of phase 1. In phase 2, it will be part of a span AB and changes to a positive moment. First, it will increase and then decrease during phase 2. At the end of the launch, it will again become a support joint and will be equal to its starting value.

$$\frac{M_J}{qL^2} = \frac{R_A}{qL}(1-\alpha) - \frac{1}{2}\frac{q_n}{q}\left(\frac{L_n}{L}\right)^2 \qquad (3.22)$$

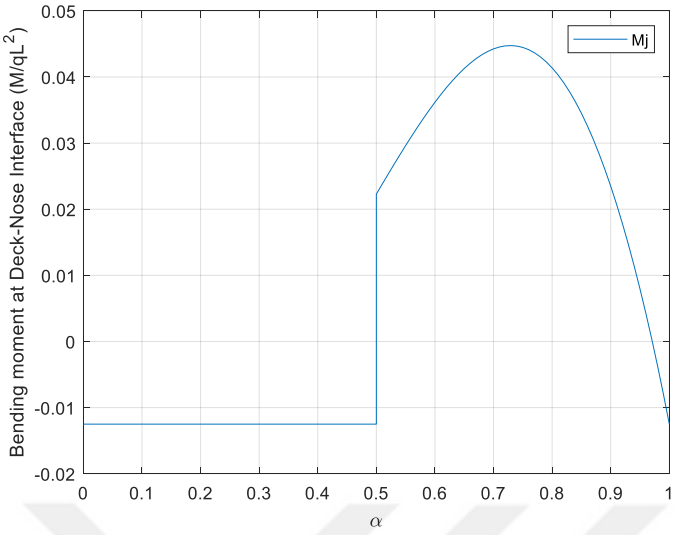

Figure 3.13. Bending Moment on Node-Deck Interface during launch (α_L =0.5 α_q =0.1 α_{EI} =0.2)

3.1.1.3 Effects of parameter changes on moments

Three main parameters affect the moment and shear forces on supports and spans: relative length (α_L), unit weight (α_q), and stiffness (α_{EI}) of the launching nose. Figure 3.14 shows the effects of changes on relative length to the M_B for fixed relative unit weight and stiffness (α_q =0.1 α_{EI} =0.2). Even though different lengths cause different moment profiles during the launching, they all converge to a similar value during phase 2. Shorter launching noses tend to have peak moment values at the end of phase 1. When the nose gets longer, this phase 1 peak value decreases, and it may be even lower than the end of the launch moment value if the nose is long enough.

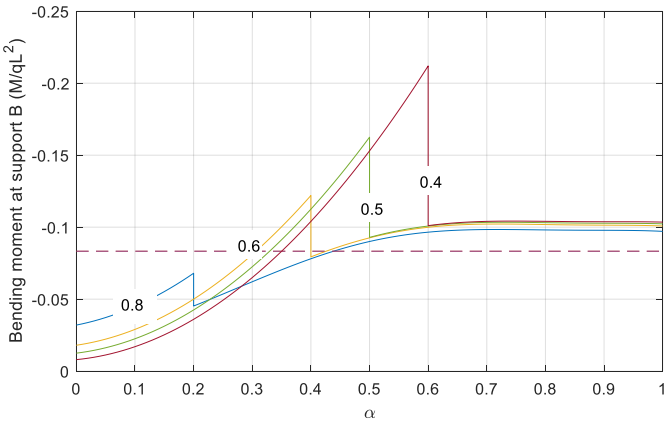

Figure 3.14. Bending Moment at Support B changes with respect to different relative lengths (α_q =0.1 α_{EI} =0.2)

Figure 3.15 shows a similar moment change graph for support C. Its behavior is like the opposite of support B, but the governing moment tends to occur at the start of the launch. Relative length change only causes minor changes on this maximum value.

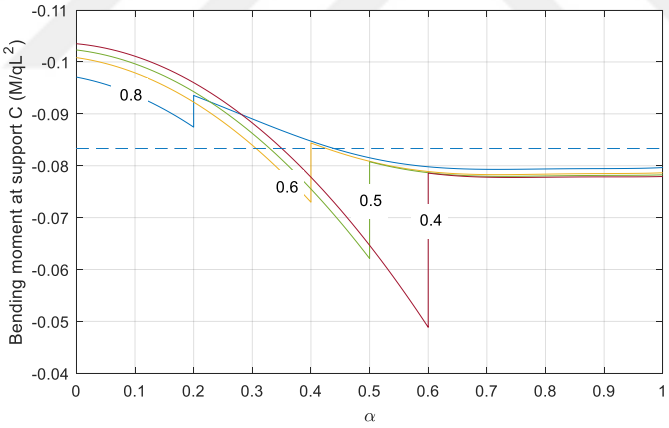

Figure 3.15. Bending Moment at Support C changes with respect to different relative lengths (α_q =0.1 α_{EI} =0.2)

Figure 3.16 shows the effects of change in relative unit weight on the support B for the same relative length and stiffness values (α_L =0.1 α_{EI} =0.2). Heavier launching nose causes higher bending moments on phase 1 due to the cantilever state, but it does not cause any significant change during phase 2.

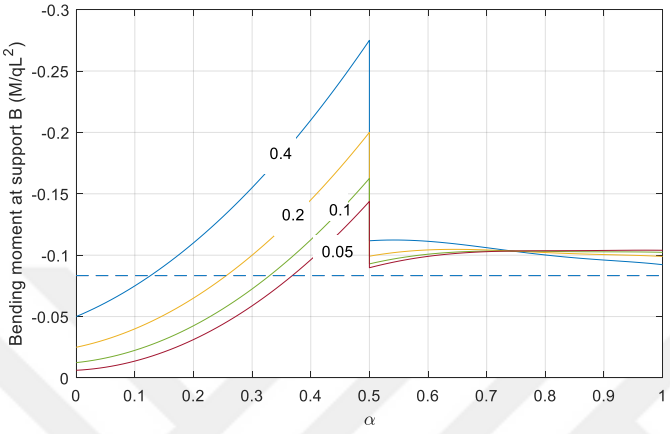

Figure 3.16. Bending Moment at Support B changes with respect to different relative unit weight (α_L =0.5 α_{EI} =0.2)

Figure 3.17 shows the relative unit weight effects for support C, where lighter launching noses cause higher bending moments.

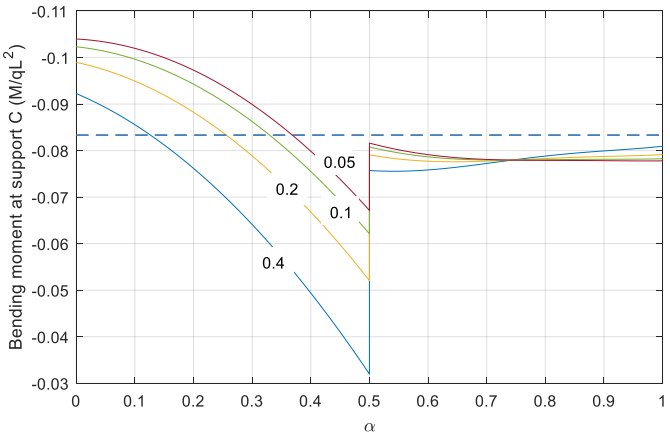

Figure 3.17. Bending Moment at Support C changes with respect to different relative unit weight (α_L =0.5 α_{EI} =0.2)

Figure 3.18 shows the effect of changes in relative bending stiffness to bending moment on support B. It does not cause any change in Phase 1. Lowering bending stiffness causes an increase on moments during phase 2, but it does not cause any change on the final end of the launch moment. Launching noses with different stiffness values converge on the same value at the end of the launch. Therefore, a launching nose with a very high stiffness value (α_{EI} =0.4 for this example) is unnecessary. Even though it causes less negative moment during phase 2, it still reaches the same final moment value as low stiffness launching noses.

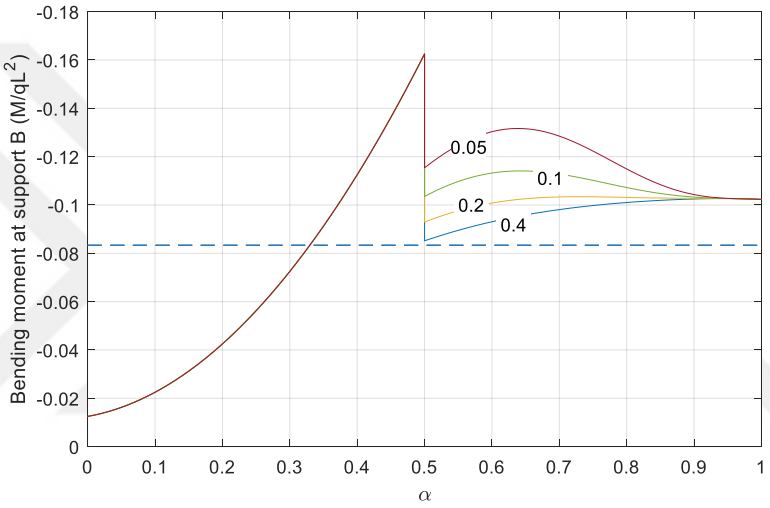

Figure 3.18. Bending Moment at Support B changes with respect to different relative bending stiffness (α_L =0.5 α_q =0.1)

Figure 3.19 shows the effects of relative bending stiffness change on the moment of support C. Higher bending stiffness causes higher negative moments on support C during phase 2; nevertheless, maximum negative moment on support C generally occurs at the start of phase 1.

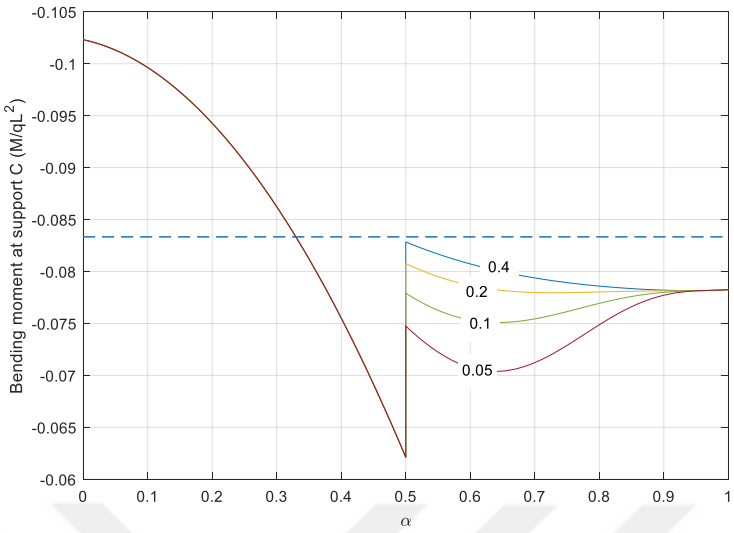

Figure 3.19. Bending Moment at Support C changes with respect to different relative bending stiffness (α_L =0.1 α_q =0.1)

3.1.2 Semi-Infinite Beam Model

The semi-infinite beam model is based on the infinite beam model. The infinite beam model assumes an infinite continuous beam with equal spans. The semi-infinite beam model also has the same assumption, but it aims to represent this behavior with a defined number of spans, making it easier to analyze. It aims to create a simple finite element model for the nose-deck behavior. This approach creates a more familiar model for the designers where they can easily understand, apply, and make necessary changes when it is required.

The semi-infinite beam model has the following assumptions (Hirmand et al., 2013):

- ILM prestressed concrete bridges are mostly consisting of box sections that have very high torsional stiffness. Therefore, the torsional moment is not critical, and sections can be considered as straight beams.
- Effects of settlement and temperature are neglected.

- Due to the cyclic nature of positive and negative bending moments during the construction phase, prestressing is concentric.
- Stiffness and unit weights of the deck and launching nose are constant through the length.
- Shear effects on the behavior and the internal forces of the deck can be neglected.
- All spans are equal in length.
- The bridge consists of a very high number of sections behind the launching span. Therefore, it can be considered as a continuous beam with infinite spans.

The above assumptions are also applied to the infinite beam model. But the semi-infinite beam model aims to express this infinite beam behavior with a less number of beams. Forces and moments during the launch primarily affect the front spans, and as we go further from the launching span, these effects diminish.

Figure 3.20 shows the rotation changes on a support point during the launching. When 3 spans are completely launched, angular displacement at the furthest point getting closer to zero, which can be expressed as a fixed support deck (Hirmand et al., 2013).

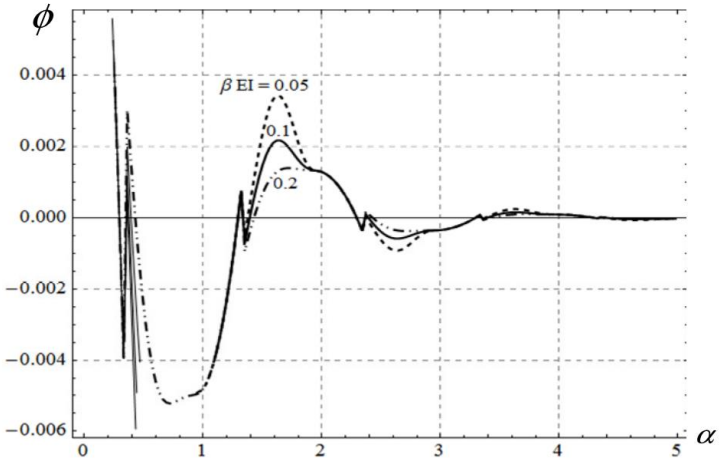

Figure 3.20. Variation of the rotation of the deck (Hirmand et al., 2013)

Thus, this infinite beam structure may be expressed as follows: one fixed support at the end, pin supports on the intervals, and cantilever at the other end (Hirmand et al., 2013). Figure 3.22 shows this idealization. But this is a supposition, and it may be incorrect; therefore, it needs to be checked. In Chapter 3.3, semi-infinite beam models are compared against the infinite beam model to understand whether they show the same behavior or not.

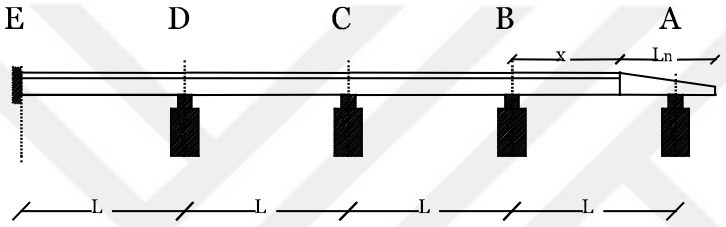

Figure 3.21. Semi-Infinite Beam Model with 3 launched spans

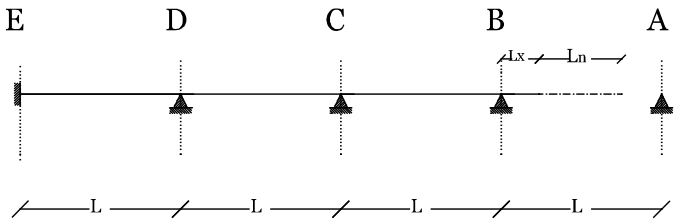

Figure 3.22. Structural idealization of Semi-Infinite Beam Model

The system may be solved easily with ordinary slope deflection equations or finite element modeling. Hirmand et al. (2013) stated that the third support behind the launching span (E) has a rotation value approximately equal to 0. Therefore, it is chosen as fixed support (Figure 3.21 and Figure 3.22).

Hirmand et al. (2013) and Shojaei et al. (2015b) 's models have 3 already launched spans behind the launching span. But there are studies that suggest 2 spans behind the launching section is sufficient. Wang et al. (2010) suggest that support D takes no effect from the stresses due to the front-end launching nose and has approximately 0 rotation, and therefore, point D can be modeled as fixed support (Figure 3.23).

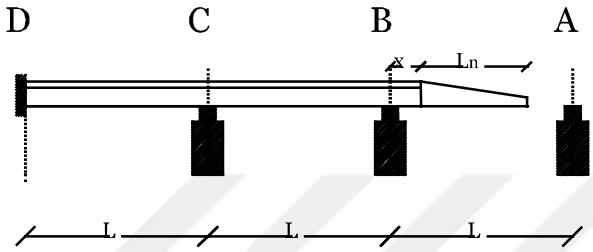

Figure 3.23. Semi-Infinite Beam Model with 2 spans behind

Both infinite and semi-infinite models assume that many sections are already launched, but this assumption is not correct for the launching of the initial sections. Therefore, a new model for the initial stages has been developed and then compared with the semi-infinite beam models in Chapter 4.

3.2 Optimization of Incrementally Launched Bridges

Engineers try to reach optimum safety, time, and cost for a given structure under defined circumstances. The incremental launching method is chosen for its advantages in these areas. While non-requirement of scaffolding decreases the cost, method's application requirements will increase the cost.

Deck sections will be under cyclic loading of both positive and negative bending moments during the launch. These loads are different from the service life loads and will cause changes in the deck cross-sections, increasing the total cost. The launching nose should be chosen to minimize these moments.

On the other hand, the launching nose itself will be an extra cost, and therefore, engineers will try to design a lightweight, shorter nose. An optimum launching nose should reduce the moments on the deck and should not be an overdesign.

In this chapter, various optimization studies focused on dimensioning of the launching nose are explained. These methods assume that many sections are already launched. In other words, they are based on the advanced stage models explained in the previous chapters. Also, none of these models are considered the deflection of the cantilever launching nose as a parameter.

3.2.1 Trial and Error Method

Rosignoli (1998) used a trial and error method to optimize the launching nose based on the infinite beam model. As explained in the previous chapter, support B is generally considered as the most critical point for a system with many equal spans. Early studies on the optimization focused on minimizing the negative moment on B (Rosignoli, 1998). The moment diagram of support B for chosen parameters (α_L =0.5 α_q =0.1) with different relative stiffnesses is shown in Figure 3.24.

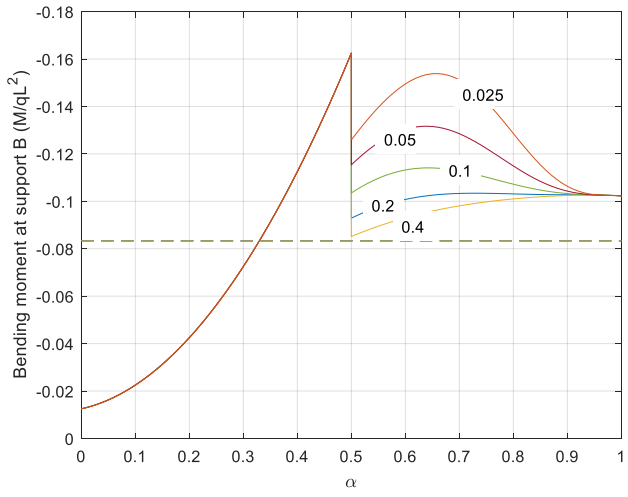

Figure 3.24. Bending Moment at Support B for different relative bending stiffnesses (α_L =0.5 α_q =0.1)

For this situation, the peak moment occurred at the end of phase 1, and after that, the bending moment is less than the peak value up to the end of the launch. It is known that phase 1 moment values are significantly depending on launching nose length. To decrease the peak value of phase 1, the launching nose length is increased (Figure 3.25). The relative length of 0.8 is chosen for this new configuration.

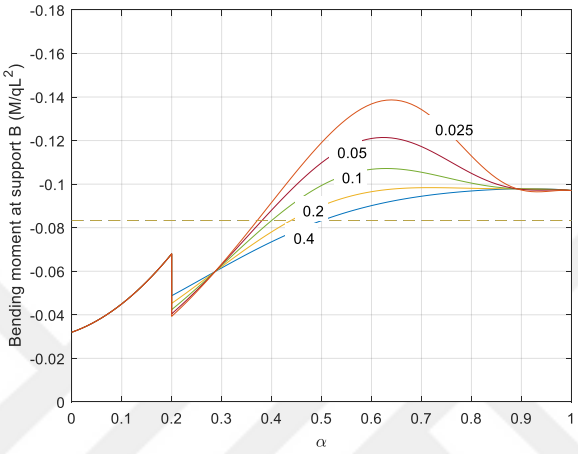

Figure 3.25. Bending Moment at Support B for different relative bending stiffnesses (α_L =0.8 α_q =0.1)

Longer launching nose causes a decrease on the maximum moment on phase 1. Then the maximum negative bending moment occurs in phase 2. As shown in Figure 3.25, moments in phase 2 are significantly dependent on the launching nose's relative stiffness up to 85% of the launch. In the last portion, launching noses with different bending stiffnesses reach the same moment values. A higher value of relative stiffness is better in this situation, but a stiffness ratio higher than 0.2 would be overdesign. A launching nose with a relative stiffness ratio whose peak corresponds to the end of the launch moment should be chosen to have an optimum design in phase 2. In this case, it is α_{EI} =0.2.

Also, in the current configuration, the launching nose is unnecessarily long (overdesigned). Launching can be shortened until the first and second peaks are equal (Figure 3.26) with the trial and error method (Rosignoli, 1998).

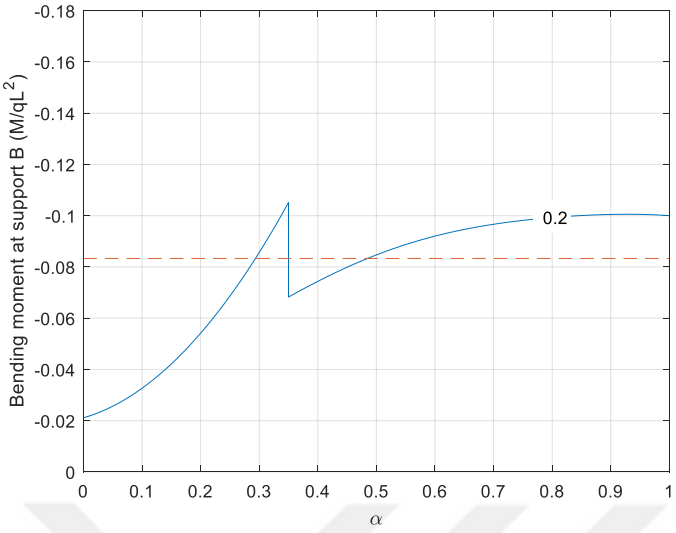

Figure 3.26. Bending Moment at Support B (α_L =0.65 α_q =0.1 α_{EI} =0.2)

Figure 3.26 shows an optimum design of a launching nose for a chosen fixed unit weight ratio (α_q =0.1). To summarize, an optimum launching nose satisfies the equalization of contact (end of phase 1) and end of launch (end of phase 2) moments (Rosignoli, 2002). Rosignoli (1998) suggested using trial and error to find optimum values. Figure 3.27 shows optimum relative lengths with respect to different relative unit weight values. Of course, this optimization is limited by real-life material behavior and design considerations. Launching nose unit weight has the following constraints (Rosignoli, 1998):

$$q_n = kL_n^2$$

$0.012 < k < 0.02$ for highway bridges (3.23)

$0.018 < k < 0.03$ for railway bridges (3.24)

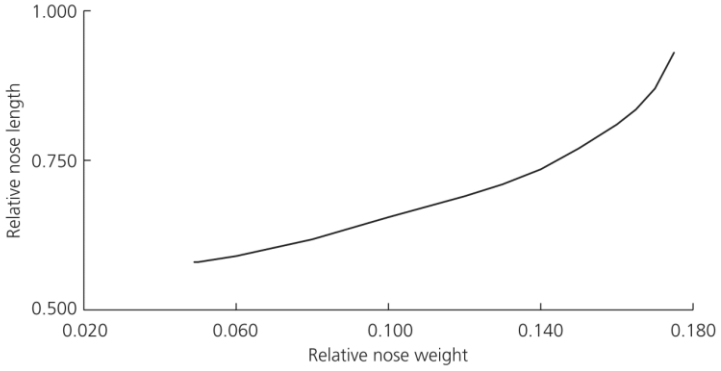

Figure 3.27. Optimal relative length for the negative bending moment as relative unit weight changes (Rosignoli, 2014)

3.2.2 Analytical Method

Apart from the trial and error method, an analytical approach has also been developed (Hirmand et al., 2013; Wang et al., 2010). These methods use the semi-infinite beam model. Formulas for M_{B1} and M_{B2} are already known. The target is to find other parameters when M_{B1} at the end of phase 1 (3.25) is equal to M_{B2} at the end of the launch (3.26). Following equations are derived (Wang et al., 2010):

$$M_{B1}(x = 1 - L_n) = \left(0.5\alpha_L\alpha_q + \alpha_L\alpha_q(1 - \alpha_L) + 0.5(1 - \alpha_L)^2\right)qL^2 \quad (3.25)$$

$$M_{B2}(x = 1) = \left(0.134\alpha_L^2\alpha_q - 0.106\right)qL^2 \quad (3.26)$$

When equations (3.25) and (3.26) are solved together, the result is the best relative length with respect to relative unit weight (3.27) (Wang et al., 2010). Figure 3.28 shows the graph of this equation.

$$\alpha_{L,best} = \frac{\sqrt{\alpha_q^2 - 1.42318\alpha_q + 0.212} + \alpha_q - 1}{0.732\alpha_q - 1} \quad (3.27)$$

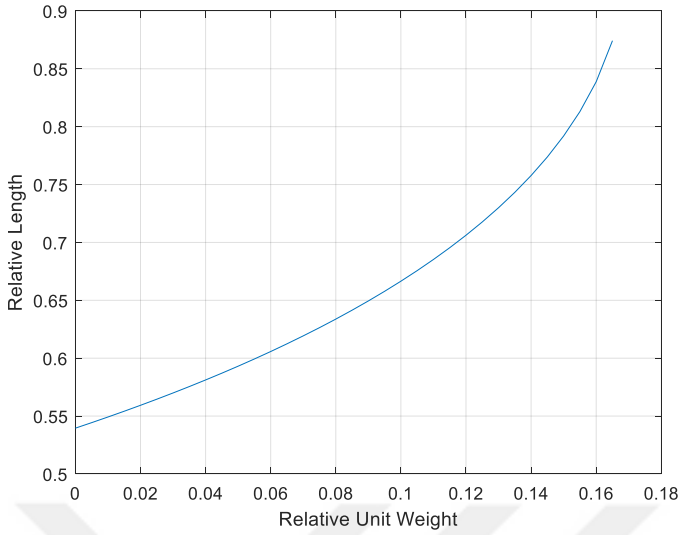

Figure 3.28. Relationship between optimized relative length and relative unit weight of the launching nose

Equation (3.28) and Figure 3.29 shows a similar equation from Hirmand et al. (2013). In this equation, α_q is written in terms of α_L. However, both of these equations do not consider the possible phase 2 peaks due to the low relative stiffness ratio (Figure 3.25). To use these equations, relative stiffness should be chosen such that it will not create a bending moment value during phase 2 higher than the end of launch bending moment.

$$\alpha_{q,best} = \frac{0.3942 - \alpha_L + 0.5\alpha_L^2}{(0.3654\alpha_L - 1)\alpha_L} \tag{3.28}$$

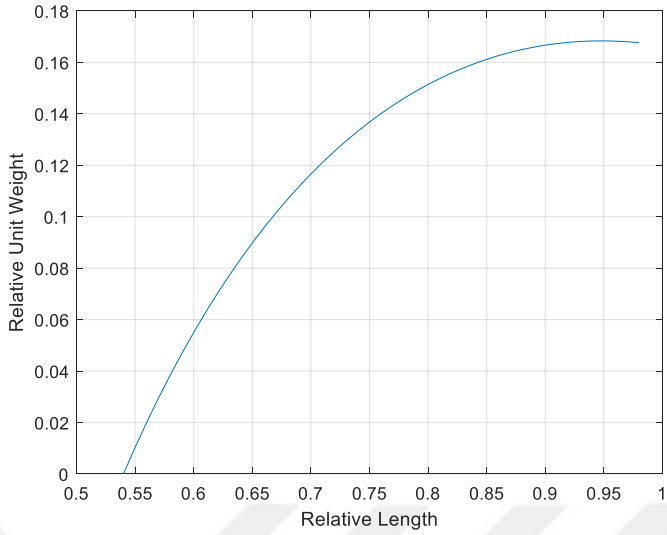

Figure 3.29. Relationship between optimized relative unit weight and relative length of the launching nose

3.2.3 Numerical Method

Besides basic trial & error and analytical methods, more advanced numerical optimization methods are also developed to find the optimum launching nose design in incrementally launched bridges. Previous methods were focused on finding the best situation via equality of bending moment of support B at the end of phase 1 ($x=1-L_n$) and end of phase 2 ($x=L$) while keeping phase 2 intermediate moments less than this equal optimum moment value. However, Fontan et al. (2010) state that this is a heuristic supposition, and it may be incorrect; therefore, it needs to be tested with other methods. Fontan et al. (2010) used the method of the feasible direction to solve this phenomenon with the following objective function (3.29), which focused on reaching the minimum bending moments without any supposition.

$$\min \max \left[M_{B1}(1-a_L), M_{B2}(a)\right] \tag{3.29}$$

With this method, they reached a smaller M_B value, but the result was unrealistic. Required launching nose length is equal to span length ($\alpha_L = 1$); it should have lower

unity weight value (α_{EI}=0.171) and relative stiffness (α_{EI}=0.273). Figure 3.30 shows the result of this optimization. It is known that a long launching nose requires higher values of relative stiffness and unity weight (Fontan et al., 2010).

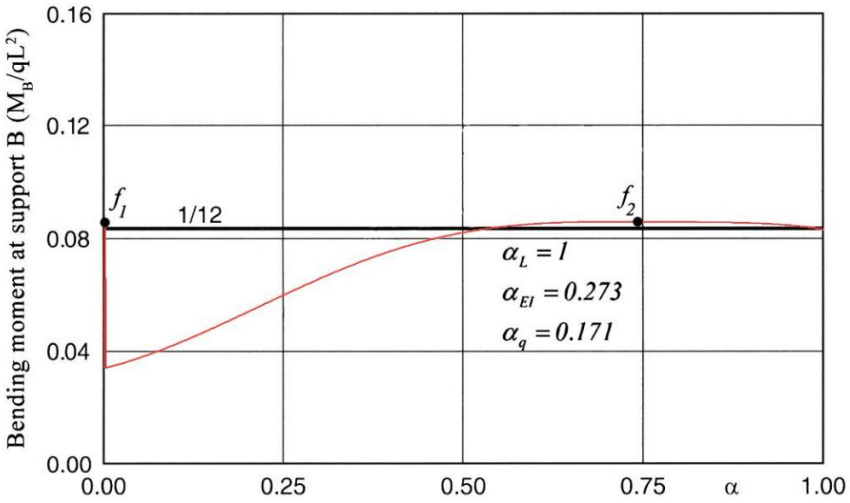

Figure 3.30. Optimum evolution of M_B (Fontan et al., 2010)

On their trials, they have also encountered results where support C has higher negative bending moment values than support B for very high relative lengths. Therefore, Mc is also added to the objective function (3.30).

$$\text{Min max } [M_{B1}(1-a_L), M_{B2}(a), M_{C1}(0), M_{C2}(a)] \qquad (3.30)$$

Later on, they added span moments to the objective functions (3.31), but they were not determining factors for chosen parameters (Fontan et al., 2010). Constraints for the relation between relative length and relative unit weight (Equation (3.23) and (3.24)) are added based on Rosignoli (1998). Method of feasible direction with additional objective functions and constraints is more useful than the other methods because of its ability to check more than one condition. However, the lack of relation between relative stiffness and other parameters might cause unrealistic results.

$$\min \max \left[\frac{M_{B1}(1-a_L)}{W_s}, \frac{M_{B2}(a)}{W_s}, \frac{M_{C1}(0)}{W_s}, \frac{M_{C2}(a)}{W_s}, -\frac{M_{AB2}(a)}{W_i}, -\frac{M_{BC1}(0)}{W_i}, -\frac{M_{BC2}(a)}{W_i} \right] \quad (3.31)$$

3.3 Comparison of the Advanced Stage Analysis Models

In this chapter, the analysis model for the current advanced stage semi-infinite beam model is explained and compared with the infinite beam model to understand whether the semi-infinite beam model matches with the infinite beam assumption or not.

3.3.1 Development of FEM Analysis for the Semi-Infinite Beam Model

FEM analysis code is developed based on the semi-infinite beam model. In summary, the code structure is as follows:

- Form element stiffness matrices [K_{el}]
- Form element force matrices based on fixed end moments [F_{el}]
- Assemble global stiffness and force matrices [F_g] [K_G]
- Solve global force equations to find deflections [F_g]=[K_G]*[u]
- Find member end forces using local force equations [F_{el}]=[K_{el}]*[u]

A system with boundary conditions is required for structural calculations. Figure 3.32 shows an example of a semi-infinite beam model of phase 1, before the launching nose reaches the target pier. It is a continuous beam under its own dead load supported by the piers. Uplift will not occur on any support point even under the worst conditions; maximum cantilever weight is not more than the previous spans. Therefore, all support points are modeled as restricted against the vertical movement. The rearward joint is treated as a fixed joint due to its small rotation

(Hirmand et al., 2013). Figure 3.33 shows the structural idealization of the semi-infinite beam model. Other support points allowing rotations are defined as pin supports.

Figure 3.31 shows the degrees of freedom of a member. Only the dead loads of the bridge deck and the launching nose are applied as external loads. The following are neglected in this formulations: temperature effects, settlements of piers, and shear effects (Hirmand et al., 2013).

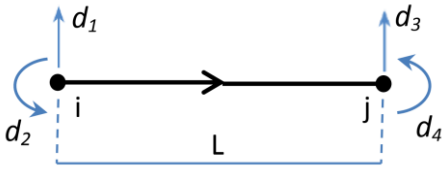

Figure 3.31. Degrees of freedom of a member

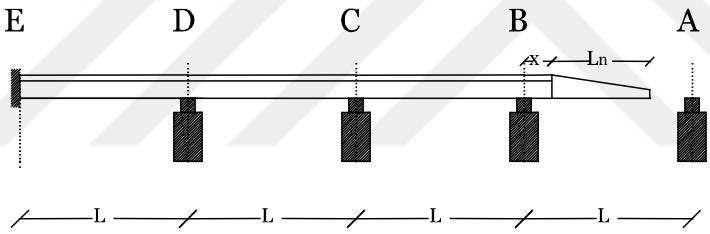

Figure 3.32. Semi-Infinite Beam Model with 3 launched spans – Phase 1

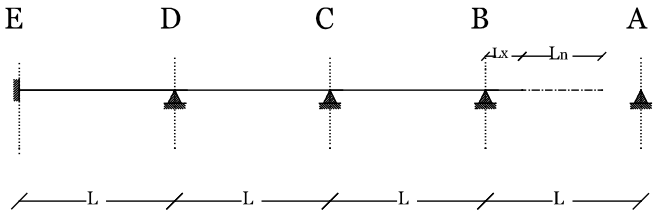

Figure 3.33. Structural idealization of Semi-Infinite Beam Model – Phase 1

In current models in the literature, the furthest cantilever part of the launching nose (Figure 3.32) was not modeled and expressed only as its external moments and force effects. Therefore, these semi-infinite beam models do not give any information on the deflection of the launching nose. In this thesis, that part of the launching nose is also modeled to calculate the deflection of the launching nose. A launching nose is assumed to have constant thickness and unit weight over the length. This assumption corresponds to current models' assumptions (Rosignoli, 1998; Shojaei et al., 2015).

Symbols used in this chapter are:

- S: Bending stiffness of the deck
- S_n: Bending stiffness of the launching nose
- q: Unit weight of the deck
- q_n: Unit weight of the launching nose
- L: Span length
- L_x: Launched span length
- L_n: Launching nose length

Element stiffness matrices of a regular deck section and phase 1 cantilever launching nose are defined and showed in (3.32), (3.33), and (3.34). Stiffness matrices of other elements are also prepared in similar manners.

$$K_{deck} = \begin{bmatrix} \frac{12*S}{L^3} & \frac{6*S}{L^2} & -\frac{12*S}{L^3} & \frac{6*S}{L^2} \\ \frac{6*S}{L^2} & \frac{4*S}{L} & -\frac{6*S}{L^2} & \frac{2*S}{L} \\ -\frac{12*S}{L^3} & -\frac{6*S}{L^2} & \frac{12*S}{L^3} & -\frac{6*S}{L^2} \\ \frac{6*S}{L^2} & \frac{2*S}{L} & -\frac{6*S}{L^2} & \frac{4*S}{L} \end{bmatrix} \quad (3.32)$$

$$K_{\text{launched span}} = \begin{bmatrix} \frac{12*S}{L_x^3} & \frac{6*S}{L_x^2} & -\frac{12*S}{L_x^3} & \frac{6*S}{L_x^2} \\ \frac{6*S}{L_x^2} & \frac{4*S}{L_x} & -\frac{6*S}{L_x^2} & \frac{2*S}{L_x} \\ -\frac{12*S}{L_x^3} & -\frac{6*S}{L_x^2} & \frac{12*S}{L_x^3} & -\frac{6*S}{L_x^2} \\ \frac{6*S}{L_x^2} & \frac{2*S}{L_x} & -\frac{6*S}{L_x^2} & \frac{4*S}{L_x} \end{bmatrix} \quad (3.33)$$

$$K_{\text{launching nose}} = \begin{bmatrix} \frac{12*S_n}{L_n^3} & \frac{6*S_n}{L_n^2} & -\frac{12*S_n}{L_n^3} & \frac{6*S_n}{L_n^2} \\ \frac{6*S_n}{L_n^2} & \frac{4*S_n}{L_n} & -\frac{6*S_n}{L_n^2} & \frac{2*S_n}{L_n} \\ -\frac{12*S_n}{L_n^3} & -\frac{6*S_n}{L_n^2} & \frac{12*S_n}{L_n^3} & -\frac{6*S_n}{{L_n}^2} \\ \frac{6*S_n}{L_n^2} & \frac{2*S_n}{L_n} & -\frac{6*S_n}{L_n^2} & \frac{4*S_n}{L_n} \end{bmatrix} \quad (3.34)$$

During the launching phase of the incremental launch, each part only carries its own weight. The system does not have any external loads. Fixed end forces and moments due to these self-weights are calculated for each element showed in (3.35), (3.36), and (3.37).

$$F^{\text{Fixed}}{}_{\text{deck}} = \begin{bmatrix} \frac{L*q}{2} \\ \frac{L^2*q}{12} \\ \frac{L*q}{2} \\ -\frac{L^2*q}{12} \end{bmatrix} \quad (3.35)$$

$$F^{\text{Fixed}}{}_{\text{launched span}} = \begin{bmatrix} \frac{L_x*q}{2} \\ \frac{L_x^2*q}{12} \\ \frac{L_x*q}{2} \\ -\frac{L_x^2*q}{12} \end{bmatrix} \quad (3.36)$$

$$F^{\text{Fixed}}{}_{\text{launching nose}} = \begin{bmatrix} \frac{L_n * q}{2} \\ \frac{L_n^2 * q}{12} \\ \frac{L_n * q}{2} \\ -\frac{L_n^2 * q}{12} \end{bmatrix} \tag{3.37}$$

The global stiffness matrix (Figure 3.34) and forces matrix (3.38) are assembled based on element stiffness and fixed end forces matrices.

$$F^{\text{Fixed}}{}_{\text{global}} = \begin{bmatrix} \frac{L * q}{2} \\ \frac{L^2 * q}{12} \\ L * q \\ 0 \\ L * q \\ 0 \\ \frac{L * q}{2} + \frac{L_x * q}{2} \\ \frac{q * L_x^2}{12} - \frac{L^2 * q}{12} \\ \frac{L_x * q}{2} + \frac{L_n * q_n}{2} \\ \frac{q_n * L_n^2}{12} - \frac{L_x^2 * q}{12} \\ \frac{L_n * q_n}{2} \\ -\frac{L_n^2 * q_n}{12} \end{bmatrix} \tag{3.38}$$

$$\begin{bmatrix} \frac{12*S}{L^3} & \frac{6*S}{L^2} & -\frac{12*S}{L^3} & \frac{6*S}{L^2} & 0 & 0 & 0 & 0 & 0 & 0 & 0 & 0 \\ \frac{6*S}{L^2} & \frac{4*S}{L} & -\frac{6*S}{L^2} & \frac{2*S}{L} & 0 & 0 & 0 & 0 & 0 & 0 & 0 & 0 \\ -\frac{12*S}{L^3} & -\frac{6*S}{L^2} & \frac{24*S}{L^3} & 0 & -\frac{12*S}{L^3} & \frac{6*S}{L^2} & 0 & 0 & 0 & 0 & 0 & 0 \\ \frac{6*S}{L^2} & \frac{2*S}{L} & 0 & \frac{8*S}{L} & -\frac{6*S}{L^2} & \frac{2*S}{L} & 0 & 0 & 0 & 0 & 0 & 0 \\ 0 & 0 & -\frac{12*S}{L^3} & -\frac{6*S}{L^2} & \frac{24*S}{L^3} & 0 & -\frac{12*S}{L^3} & \frac{6*S}{L^2} & 0 & 0 & 0 & 0 \\ 0 & 0 & \frac{6*S}{L^2} & \frac{2*S}{L} & 0 & \frac{8*S}{L} & -\frac{6*S}{L^2} & \frac{2*S}{L} & 0 & 0 & 0 & 0 \\ 0 & 0 & 0 & 0 & -\frac{12*S}{L^3} & -\frac{6*S}{L^2} & \frac{12*S}{L^3}+\frac{12*S}{Lx^3} & \frac{6*S}{Lx^2}-\frac{6*S}{L^2} & -\frac{12*S}{Lx^3} & \frac{6*S}{Lx^2} & 0 & 0 \\ 0 & 0 & 0 & 0 & \frac{6*S}{L^2} & \frac{2*S}{L} & \frac{6*S}{Lx^2}-\frac{6*S}{L^2} & \frac{4*S}{L}+\frac{4*S}{Lx} & -\frac{6*S}{Lx^2} & \frac{2*S}{Lx} & 0 & 0 \\ 0 & 0 & 0 & 0 & 0 & 0 & -\frac{12*S}{Lx^3} & -\frac{6*S}{Lx^2} & \frac{12*S}{Lx^3}+\frac{12*Sn}{Ln^3} & \frac{6*Sn}{Ln^2}-\frac{6*S}{Lx^2} & -\frac{12*Sn}{Ln^3} & \frac{6*Sn}{Ln^2} \\ 0 & 0 & 0 & 0 & 0 & 0 & \frac{6*S}{Lx^2} & \frac{2*S}{Lx} & \frac{6*Sn}{Ln^2}-\frac{6*S}{Lx^2} & \frac{4*S}{Lx}+\frac{4*Sn}{Ln} & -\frac{6*Sn}{Ln^2} & \frac{2*Sn}{Ln} \\ 0 & 0 & 0 & 0 & 0 & 0 & 0 & 0 & -\frac{12*Sn}{Ln^3} & -\frac{6*Sn}{Ln^2} & \frac{12*Sn}{Ln^3} & -\frac{6*Sn}{Ln^2} \\ 0 & 0 & 0 & 0 & 0 & 0 & 0 & 0 & \frac{6*Sn}{Ln^2} & \frac{2*Sn}{Ln} & -\frac{6*Sn}{Ln^2} & \frac{4*Sn}{Ln} \end{bmatrix}$$

Figure 3.34. Global Stiffness Matrix – Phase 1

$$F - F^{Fixed} = K*U \tag{3.39}$$

The stiffness equation (3.39) is solved using symbolic parameters. Symbolic parameters are used for representative solutions in MATLAB. With this method, we can get the exact equations without using any real or arbitrary value. The results will be in terms of parameters only. After the general stiffness matrix equation solution, results are used to solve the element stiffness equations to get member end forces.

As a result, the equation of all element nodes' deflections, rotations, forces, and bending moments are derived. These equations are based on element dimensions, materials, and launching increments. If the classical methods were used, it would require a complete rerun of the software to solve each increment step. But with this method, only one analytical solution for each phase is enough. Now all force and deflection equations are presented in simple analytical form.

Assign values to each parameter is enough to get any solution. In that part, the launching step (x) is defined as an array (0 to L) with the size of 100. Using element-wise calculation between x and other parameters will give all results for each increment step of the launch without using any loop.

Furthest support point A is not effective in phase 1, but when the launching nose reaches support A at the end of phase 1, this support point also became a part of the system. Therefore, behavior changes completely in phase 2. Figure 3.35 shows the configuration of phase 2.

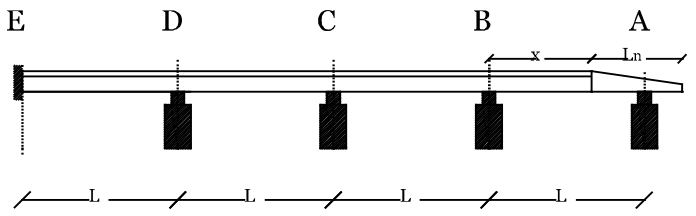

Figure 3.35. Semi-Infinite Beam Model with 3 launched spans – phase 2

A new model is prepared for phase 2. Support A is added as pin support (Figure 3.36), and the launching nose element is divided into two: launching nose behind the support A and cantilever launching nose part in front of support A. Stiffness and force matrices of the decks are the same but launching nose matrices are changed. New stiffness matrices are shown in (3.40) and (3.41). New fixed end moment matrices are shown in (3.42) and (3.43).

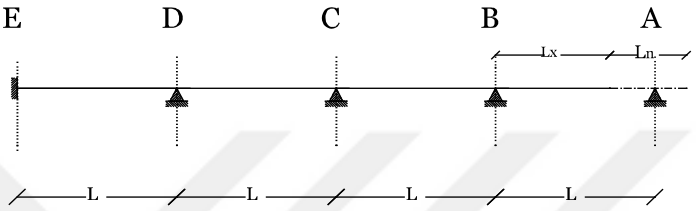

Figure 3.36. Structural idealization of Semi-Infinite Beam Model - phase 2

$$K_{\substack{\text{launching}\\ \text{nose (1)}}} = \begin{bmatrix} \frac{12 * S_n}{(L - L_x)^3} & \frac{6 * S_n}{(L - L_x)^2} & -\frac{12 * S_n}{(L - L_x)^3} & \frac{6 * S_n}{(L - L_x)^2} \\ \frac{6 * S_n}{(L - L_x)^2} & \frac{4 * S_n}{L - L_x} & -\frac{6 * S_n}{(L - L_x)^2} & \frac{2 * S_n}{L - L_x} \\ -\frac{12 * S_n}{(L - L_x)^3} & -\frac{6 * S_n}{(L - L_x)^2} & \frac{12 * S_n}{(L - L_x)^3} & -\frac{6 * S_n}{(L - L_x)^2} \\ \frac{6 * S_n}{(L - L_x)^2} & \frac{2 * S_n}{L - L_x} & -\frac{6 * S_n}{(L - L_x)^2} & \frac{4 * S_n}{L - L_x} \end{bmatrix} \quad (3.40)$$

$$K_{\substack{\text{launching}\\ \text{nose (2)}}} = \begin{bmatrix} \frac{12 * S_n}{(L_n - L + L_x)^3} & \frac{6 * S_n}{(L_n - L + L_x)^2} & -\frac{12 * S_n}{(L_n - L + L_x)^3} & \frac{6 * S_n}{(L_n - L + L_x)^2} \\ \frac{6 * S_n}{(L_n - L + L_x)^2} & \frac{4 * S_n}{L_n - L + L_x} & -\frac{6 * Sn}{(L_n - L + L_x)^2} & \frac{2 * Sn}{L_n - L + L_x} \\ -\frac{12 * S_n}{(L_n - L + L_x)^3} & -\frac{6 * S_n}{(L_n - L + L_x)^2} & \frac{12 * Sn}{(L_n - L + L_x)^3} & -\frac{6 * S_n}{(L_n - L + L_x)^2} \\ \frac{6 * S_n}{(L_n - L + L_x)^2} & \frac{2 * Sn}{L_n - L + L_x} & -\frac{6 * S_n}{(L_n - L + L_x)^2} & \frac{4 * S_n}{L_n - L + L_x} \end{bmatrix} \quad (3.41)$$

(3.42)

$$F^{Fixed}{}_{launching\ nose\ (1)=} = \begin{bmatrix} \frac{q_n * (L - L_x)}{2} \\ \frac{q_n * (L - L_x)^2}{12} \\ \frac{q_n * (L - L_x)}{2} \\ -\frac{q_n * (L - L_x)^2}{12} \end{bmatrix}$$

$$F^{Fixed}{}_{launching\ nose\ (2)=} = \begin{bmatrix} \frac{q_n * (L_n - L + L_x)}{2} \\ \frac{q_n * (L_n - L + L_x)^2}{12} \\ \frac{q_n * (L_n - L + L_x)}{2} \\ -\frac{q_n * (L_n - L + L_x)^2}{12} \end{bmatrix} \quad (3.43)$$

Global force (3.44) and stiffness (Figure 3.37) matrices are assembled. Then the above solution process is repeated for phase 2 to get phase 2 results.

$$F^{Fixed}{}_{global} = \begin{bmatrix} \frac{L * q}{2} \\ \frac{L^2 * q}{12} \\ L * q \\ 0 \\ L * q \\ 0 \\ \frac{L * q}{2} + \frac{L_x * q}{2} \\ \frac{q * L_x^2}{12} - \frac{L^2 * q}{12} \\ \frac{L_x * q}{2} + \frac{q_n * (L - L_x)}{2} \\ \frac{q_n * (L - L_x)^2}{12} - \frac{L_x^2 * q}{12} \\ \frac{q_n * (L - L_x)}{2} + \frac{q_n * (L_n - L + Lx)}{2} \\ \frac{q_n * (L_n - L + Lx)^2}{12} - \frac{q_n * (L - L_x)^2}{12} \\ \frac{q_n * (L_n - L + Lx)}{2} \\ -\frac{q_n * (L_n - L + Lx)^2}{12} \end{bmatrix} \quad (3.44)$$

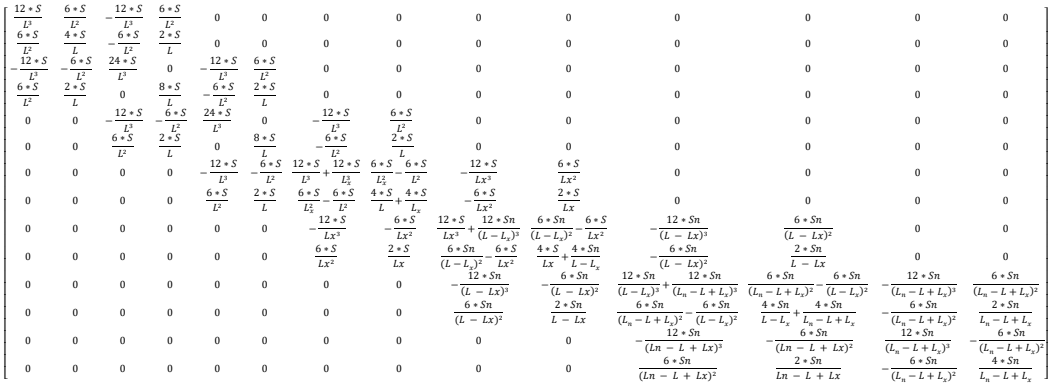

Figure 3.37. Global Stiffness Matrix – Phase 2

3.3.2 Comparison of Infinite Beam and Semi-Infinite Beam Models

All previously explained methods are aimed to explain a continuous beam structure with infinite span. The infinite beam model was the first one of these models, and other models are claimed to represent the same behavior with a defined number of spans. In this chapter, semi-infinite beam model with 2 spans launched (Figure 3.39) and 3 spans launched (Figure 3.40) are compared against the infinite beam model (Figure 3.38) to see whether they demonstrate the same behavior or not.

Infinite beam model formulations are provided (Rosignoli, 1998) and explained in Chapter 3.1.1; however, logic is explained for semi-infinite beam models (Hirmand et al., 2013; Wang et al., 2010), but detailed formulations are not provided. Therefore, an analysis code is developed and explained in the previous chapter.

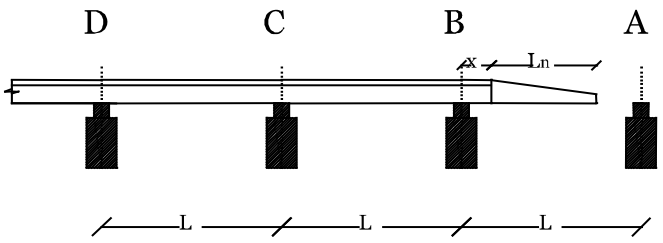

Figure 3.38. Infinite Beam Model

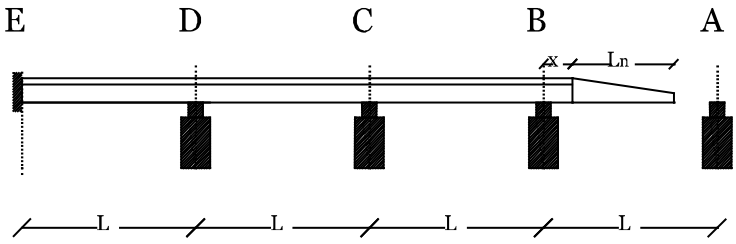

Figure 3.39. Semi-Infinite Beam Model with 3 spans behind

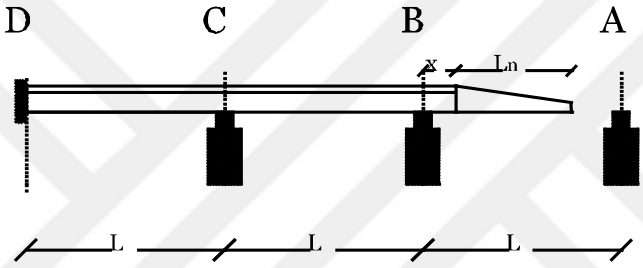

Figure 3.40. Semi-Infinite Beam Model with 2 spans behind

A comparison with only one configuration may result in an incidental match with methods. Therefore 3 different configurations are chosen to compare the infinite beam model and semi-infinite models (2 and 3 spans launched). Commonly used relative length (α_L=0.5), unit weight (α_q=0.1), and stiffness (α_{EI}=0.2) values are chosen for the normal launching nose. For shorter noses, it is assumed that shorter noses require lower unit weights; therefore, their stiffness values are also smaller. And longer launching noses are heavier with high stiffness values.

Bending moments on support B and C are used for these comparisons, which are the current optimization studies' main parameters. Selected configurations are as follows:

- α_L=0.3 α_q=0.05 α_{EI}=0.1 – Shorter, lighter and lower stiffness launching nose
- α_L=0.5 α_q=0.1 α_{EI}=0.2 – Normal launching nose
- α_L=0.8 α_q=0.2 α_{EI}=0.4 – Longer, heavier and higher stiffness launching nose

Table 3.1, Table 3.2, and Table 3.3 show the percent differences of negative bending moment on support B semi-infinite beam models (2-spans and 3-spans) against the infinite beam model for 3 different kinds of launching nose.

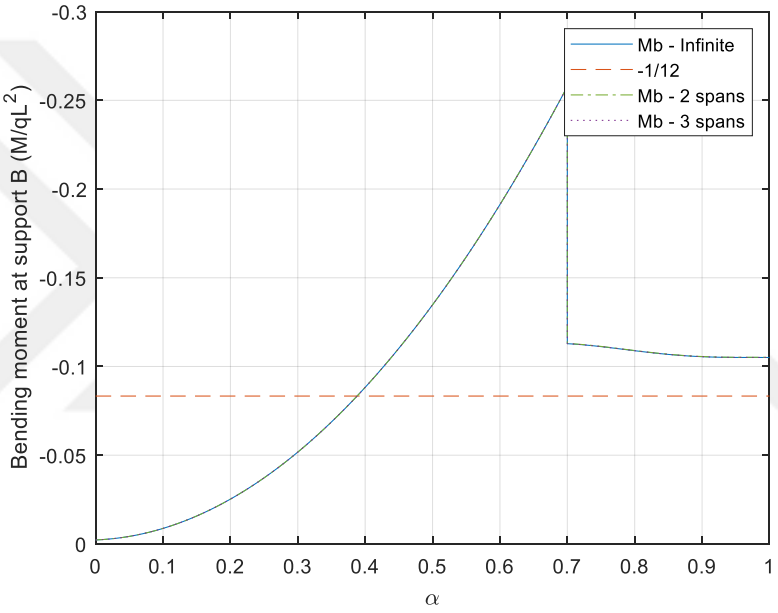

Figure 3.41. Bending Moment at Support B for different models (α_L =0.3 α_q =0.05 α_{EI} =0.1)

Table 3.1 Percent Differences of M_B for short launching nose

Compared Models	α					Max
	0	0.25	0.5	0.75	1	Moment
Semi 2 spans – Infinite	0.00%	0.00%	0.00%	0.11%	0.10%	0.00%
Semi 3 spans – Infinite	0.00%	0.00%	0.00%	0.01%	0.01%	0.00%

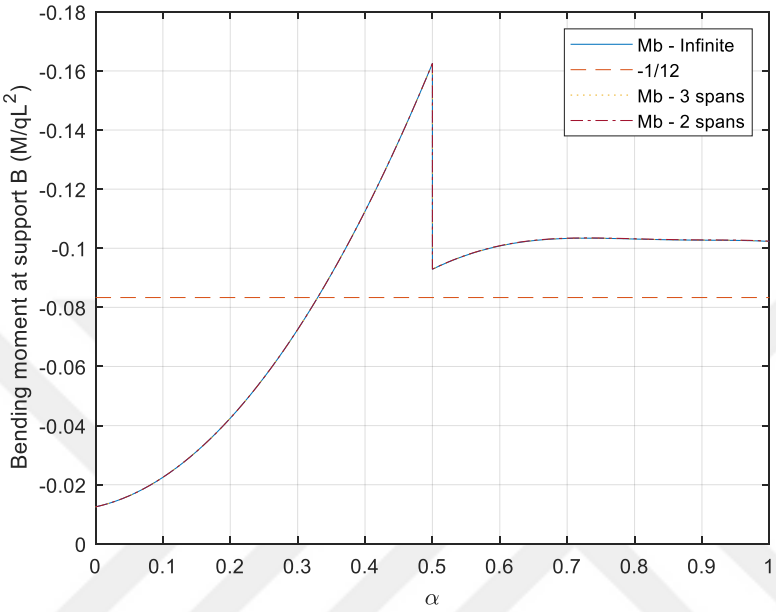

Figure 3.42. Bending Moment at Support B for different models (α_L =0.5 α_q =0.1 α_{EI} =0.2)

Table 3.2 Percent Differences of M_B for normal launching nose

Compared Models	α					Max
	0	0.25	0.5	0.75	1	Moment
Semi 2 spans – Infinite	0.00%	0.00%	0.00%	0.09%	0.09%	0.00%
Semi 3 spans – Infinite	0.00%	0.00%	0.00%	0.01%	0.01%	0.00%

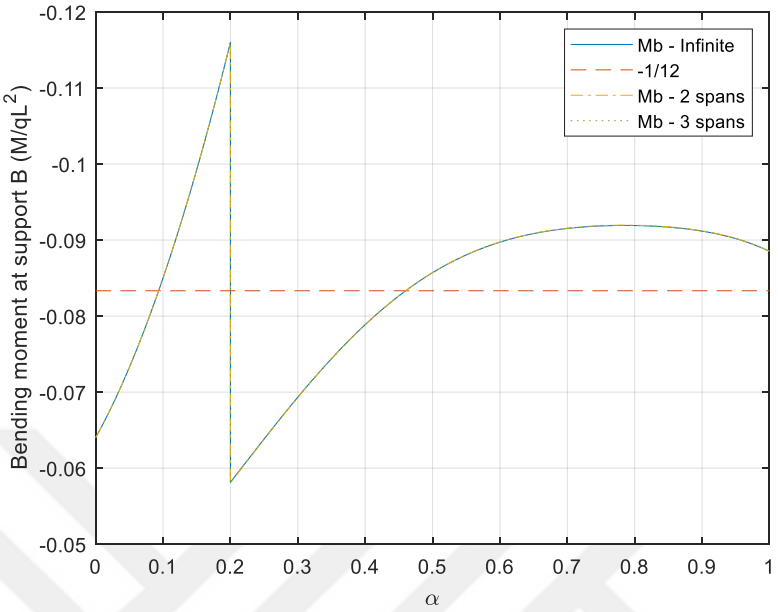

Figure 3.43. Bending Moment at Support B for different models (α_L =0.8 α_q =0.2 α_{EI} =0.4)

Table 3.3 Percent Differences of M_B for long launching nose

Compared Models	α					Max
	0	0.25	0.5	0.75	1	Moment
Semi 2 spans – Infinite	0.00%	-0.12%	0.01%	0.04%	0.03%	0.00%
Semi 3 spans – Infinite	0.00%	-0.01%	0.00%	0.00%	0.00%	0.00%

Table 3.4, Table 3.5, and Table 3.6 show the percent differences of negative bending moment on support C semi-infinite beam models (2-spans and 3-spans) against the infinite beam model for 3 different kinds of launching nose.

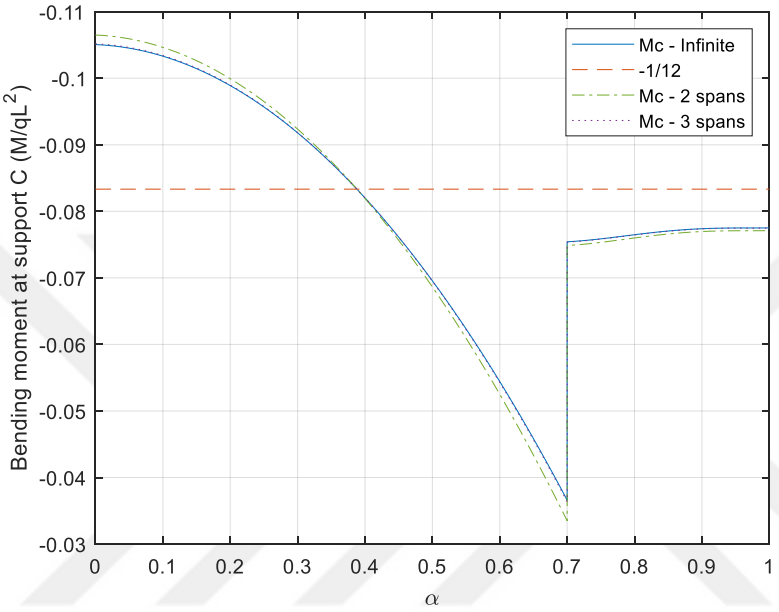

Figure 3.44. Bending Moment at Support C for different models (α_L =0.3 α_q =0.05 α_{EI} =0.1)

Table 3.4 Percent Differences of M_C for short launching nose

Compared Models	α					Max
	0	0.25	0.5	0.75	1	Moment
Semi 2 spans – Infinite	1.37%	0.86%	-1.31%	-0.70%	-0.54%	1.37%
Semi 3 spans – Infinite	0.10%	0.06%	-0.09%	-0.05%	-0.04%	0.10%

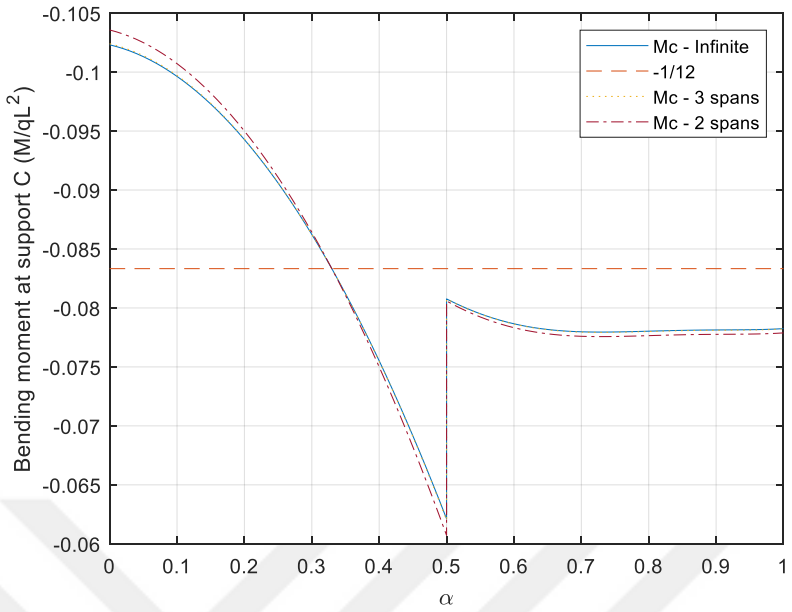

Figure 3.45. Bending Moment at Support C for different models (α_L =0.5 α_q =0.1 α_{EI} =0.2)

Table 3.5 Percent Differences of M_C for normal launching nose

Compared Models	α					Max
	0	0.25	0.5	0.75	1	Moment
Semi 2 spans – Infinite	1.23%	0.53%	-2.26%	-0.49%	-0.46%	1.23%
Semi 3 spans – Infinite	0.09%	0.04%	-0.16%	-0.04%	-0.03%	0.09%

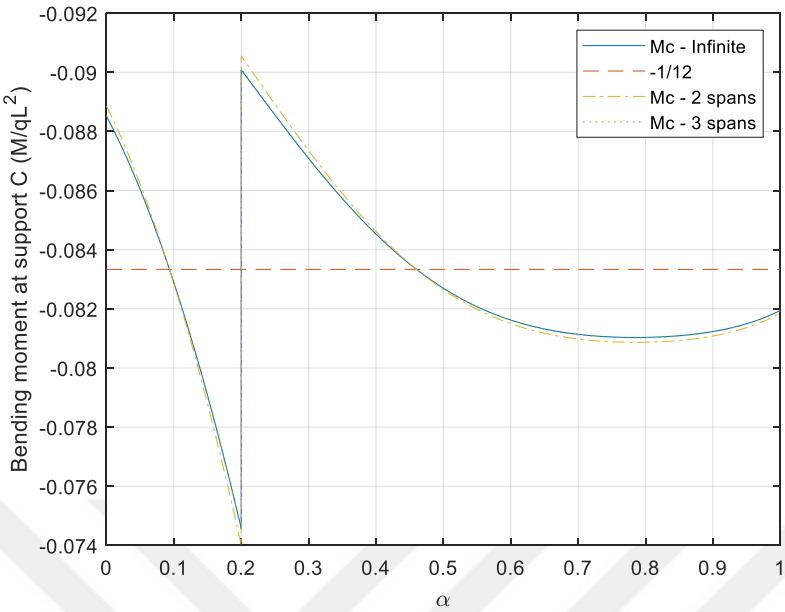

Figure 3.46. Bending Moment at Support C for different models (α_L =0.8 α_q =0.2 α_{EI} =0.4)

Table 3.6 Percent Differences of M_C for long launching nose

Compared Models	α					Max
	0	0.25	0.5	0.75	1	Moment
Semi 2 spans – Infinite	0.39%	0.44%	-0.04%	-0.20%	-0.12%	0.52%
Semi 3 spans – Infinite	0.03%	0.03%	0.00%	-0.01%	-0.01%	0.04%

As a result of these graphs and tables, we gain the following information. Bending moments on support B are in agreement for all methods. The maximum deviation during the launch is less than 1%. And the maximum moment that occurs on support B is the same for all models.

Bending moments on support C are in agreement for the infinite beam model and 3-spans semi-infinite beam model; the maximum deviation is less than 1%. 2-spans

semi-infinite beam model gives slightly higher moment results, but the difference is less than 2%.

According to these trials, we can conclude that semi-infinite beam methods give reasonable results for infinite beam behavior. The 3 spans model gives almost the same results, and the 2 spans model gives slightly higher results for support B. In the following chapters, 3 spans semi-infinite beam model will be used for representing advanced construction stage behavior.

CHAPTER 4

INITIAL STAGE ANALYSIS MODEL

A structural analysis code in MATLAB has been developed to analyze the incrementally launching bridges' initial construction stages. This code has been used to determine quick formulations for optimum design parameters of the launching nose in terms of inertia, unit weight, and length. Such equations can usually save optimization time for a designer using a standard commercial software with many time-consuming iterations. This new model also considers the deflection of the cantilever launching nose and movement of the newly casted section at the yard during the launch.

In this chapter, the new initial stage model is explained and compared with the advanced stage (semi-infinite beam) model. Finally, the effects of design parameters on the deflection of the cantilever launching nose are inspected.

4.1 Development of FEM Analysis for Initials Stages of the Launching

All the explained methods assume that many sections are already launched. These methods are good at expressing the behavior in advance stages of the construction (Hirmand et al., 2013; Rosignoli, 1998), but early stages also require examination. Therefore, a model for the analysis of the initial stages has been developed.

Semi-infinite beam models assume a rearward joint as a fixed joint based on its low rotation results (Figure 3.36). However, a real-life system does not have any fixed connection against rotation. Therefore, in a more realistic model, all joints should be assumed as pin connections (no restraint against the rotation). The newly casted span at the yard is not considered in the moment calculations on current semi-infinite models because the rearward joint is treated as fixed. In the new model, the rearward

joint has a pin connection; therefore, a new section at the yard will also be effective. This element has 2 degrees of freedom connections on both sides. The new model is expected to present a more realistic modeling of the situation. Figure 4.1 shows the idealization of this model.

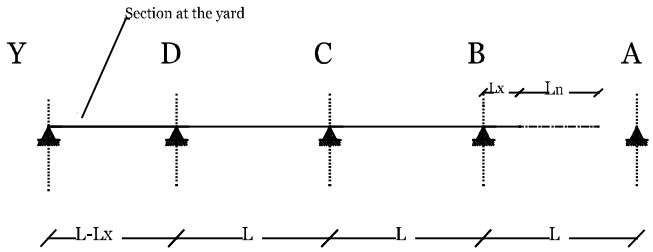

Figure 4.1. Idealization of Initial Stage Model with 2 launched span – Phase 1

The front part of the model is the same as the previous advanced stage models. It includes launched spans, launching span, and launching nose. The difference is the newly casted member in the yard. The length of this element ($L-L_x$) and the location of the rearward joint change during the launch. The length will start as a whole section (L), and it will reduce up to zero when launching is finished. Figure 4.2 and Figure 4.3 show a sketch of the launching of the 3rd span, but the same approach can be applied for other stages as well.

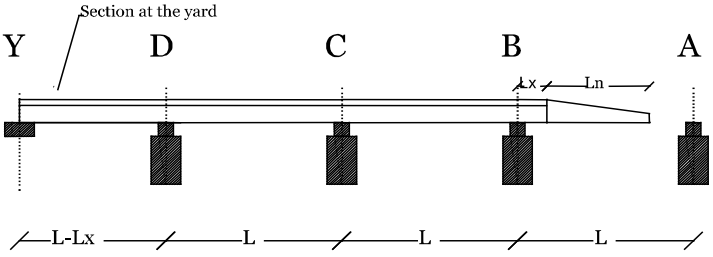

Figure 4.2. Initial Stage Model with 2 launched span – Phase 1

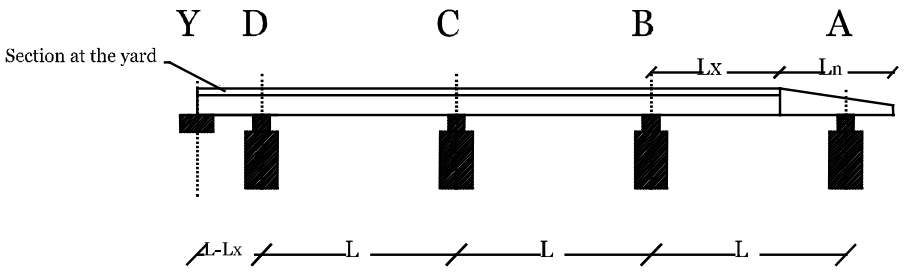

Figure 4.3. Initial Stage Model with 2 launched span – Phase 2

Many assumptions of the current advanced stage models are also applied to the initial stage model. All spans are assumed to have the same span lengths, and there are not any height differences between supports. The deck section is constant and linear through the length without any curvature.

Several effects are not considered in this method. Moments on the deck due to friction between deck girder and piers are not considered; it is assumed that low friction neoprene pads between girder and bearings will reduce these effects. The axial force that occurs on the deck is also not considered due to these low friction pads. The dead load of the deck and the launching nose are the only external loads applied to the system; wind and seismic effects are neglected. These wind and seismic effects are mainly effective in the design of the lateral bracings. Shear effects on the behavior are not considered similar to the current methods.

The newly prepared concrete deck section's stiffness matrix and fixed end moments are shown in (4.1) and (4.2). Stiffness matrices of the other deck and launching nose elements are the same as the previous models.

$$K_{\text{deck at yard}} = \begin{bmatrix} \frac{12 * S}{(L - L_x)^3} & \frac{6 * S}{(L - L_x)^2} & -\frac{12 * S}{(L - L_x)^3} & \frac{6 * S}{(L - L_x)^2} \\ \frac{6 * S}{(L - L_x)^2} & \frac{4 * S}{L - L_x} & -\frac{6 * S}{(L - L_x)^2} & \frac{2 * S}{L - L_x} \\ -\frac{12 * S}{(L - L_x)^3} & -\frac{6 * S}{(L - L_x)^2} & \frac{12 * S}{(L - L_x)^3} & -\frac{6 * S}{(L - L_x)^2} \\ \frac{6 * S}{(L - L_x)^2} & \frac{2 * S}{L - L_x} & -\frac{6 * S}{(L - L_x)^2} & \frac{4 * S}{L - L_x} \end{bmatrix} \quad (4.1)$$

$$F^{\text{Fixed}}{}_{\text{deck at yard}=} = \begin{bmatrix} \frac{q * (L - L_x)}{2} \\ \frac{q * (L - L_x)^2}{12} \\ \frac{q * (L - L_x)}{2} \\ -\frac{q * (L - L_x)^2}{12} \end{bmatrix} \quad (4.2)$$

Global force and stiffness matrices for phase 1 and phase 2 are different than each other, similar to the advanced stage methods. Equation (4.3) and Figure 4.4 shows the global force and stiffness matrices of phase 1.

$$F^{\text{Fixed}}{}_{\text{phase 1 global}} = \begin{bmatrix} \frac{q * (L - L_x)}{2} \\ \frac{q * (L - L_x)^2}{12} \\ \frac{L * q}{2} + \frac{q * (L - L_x)}{2} \\ \frac{L^2 * q}{12} - \frac{q * (L - L_x)^2}{12} \\ L * q \\ 0 \\ \frac{L * q}{2} + \frac{L_x * q}{2} \\ \frac{q * L_x^2}{12} - \frac{L^2 * q}{12} \\ \frac{L_x * q}{2} + \frac{L_n * q_n}{2} \\ \frac{q_n * L_n^2}{12} - \frac{L_x^2 * q}{12} \\ \frac{L_n * q_n}{2} \\ -\frac{L_n^2 * q_n}{12} \end{bmatrix} \quad (4.3)$$

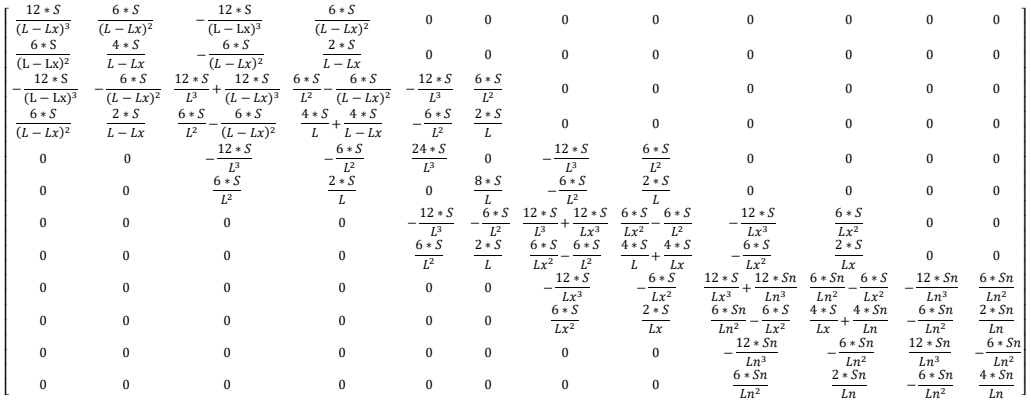

Figure 4.4. Global Stiffness Matrix – Phase 1

Equation (4.4) and Figure 4.5 shows the global force and stiffness matrices of phase 2.

$$\mathrm{F}^{\mathrm{Fixed}}{}_{\text{phase 2 global}} = \begin{bmatrix} \frac{q*(L-L_x)}{2} \\ \frac{q*(L-L_x)^2}{12} \\ \frac{L*q}{2}+\frac{q*(L-L_x)}{2} \\ \frac{L^2*q}{12}-\frac{q*(L-L_x)^2}{12} \\ \mathrm{L*q} \\ 0 \\ \frac{L*q}{2}+\frac{L_x*q}{2} \\ \frac{q*L_x^2}{12}-\frac{L^2*q}{12} \\ \frac{L_x*q}{2}+\frac{qn*(L-L_x)}{2} \\ \frac{q_n*(L-L_x)^2}{12}-\frac{Lx^2*q}{12} \\ \frac{q_n*(L-L_x)}{2}+\frac{q_n*(L_n-L+L_x)}{2} \\ \frac{q_n*(L_n-L+L_x)^2}{12}-\frac{q_n*(L-L_x)^2}{12} \\ \frac{q_n*(L_n-L+L_x)}{2} \\ -\frac{q_n*(L_n-L+L_x)^2}{12} \end{bmatrix} \tag{4.4}$$

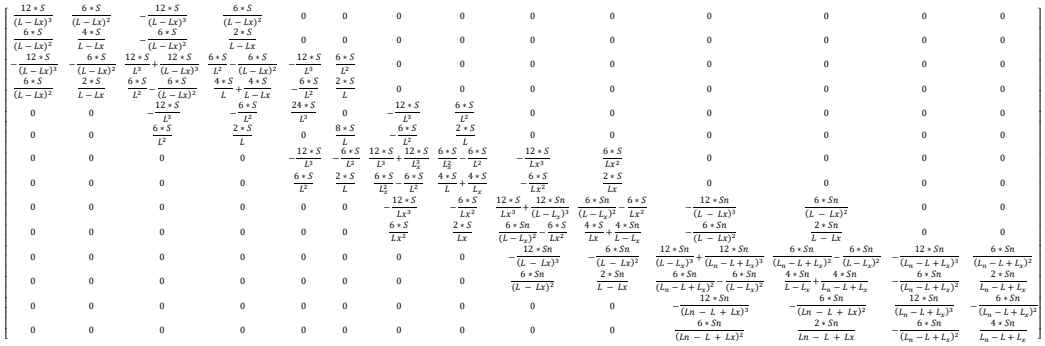

Figure 4.5. Global Stiffness Matrix – Phase 2

4.2 Comparison of Initial Stages and Advanced Stage Behaviors

Advance stage models are used in the current optimization studies, but they may leave out some of the critical cases occurring on the initial stages. In this chapter, advanced and initial stages models are compared to understand whether any critical cases occurred on initial stages or not.

For these checks, bending moment values on support B and C, shear forces on support B, and the deflections of the cantilever launching nose are compared between advanced stage behavior and initial stages (1 & 2 spans launched). The maximum moment on support B and C are the critical parameters of the current optimization studies. Three different sets of parameters are used in comparisons:

- α_L=0.3 α_q =0.05 α_{EI} =0.1 – Shorter, lighter and lower stiffness launching nose
- α_L=0.5 α_q =0.1 α_{EI} =0.2 – Normal launching nose
- α_L=0.8 α_q =0.2 α_{EI} =0.4 – Longer, heavier and higher stiffness launching nose

Table 4.1, Table 4.2, and Table 4.3 show the percent difference of negative bending moment on support B on initial stage models (1 span and 2 spans) against the advanced stage model. The moment on support B during phase 1 same for all the models because phase 1 moment is only related to the cantilever span and launching nose. Some differences were observed on phase 2. 2 spans initial stage model has 1% lower bending moment value, and 1 span initial stage model has 5% higher

bending moment value than the advanced stage. However, these differences do not affect the maximum moment. In all cases, the maximum moment on support B is the same.

Even though initial stages are not critical for the chosen launching nose parameters, it may be a critical issue for longer and lower stiffness launching noses. Long launching noses with lower bending stiffnesses tend to have critical bending value on phase 2. In that case, a 5% increase on phase 2 of 1 span initial stage model may cause problems.

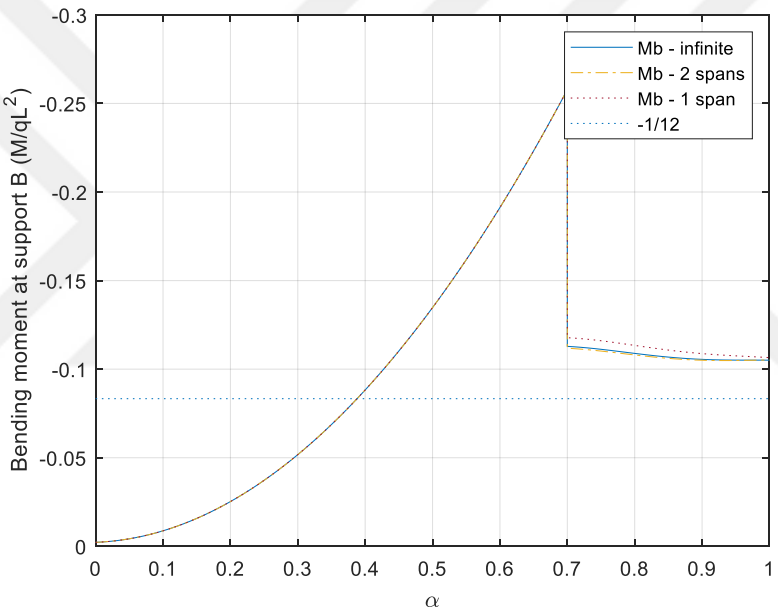

Figure 4.6. Bending Moment at Support B (α_L =0.3 α_q =0.05 α_{EI} =0.1)

Table 4.1 Percent Differences of M_B for short launching nose

Compared Models	α					Max
	0	0.25	0.5	0.75	1	Moment
2 spans – Advanced	0.00%	0.00%	0.00%	-0.89%	0.09%	0.00%
1 span – Advanced	0.00%	0.00%	0.00%	4.34%	1.36%	0.00%

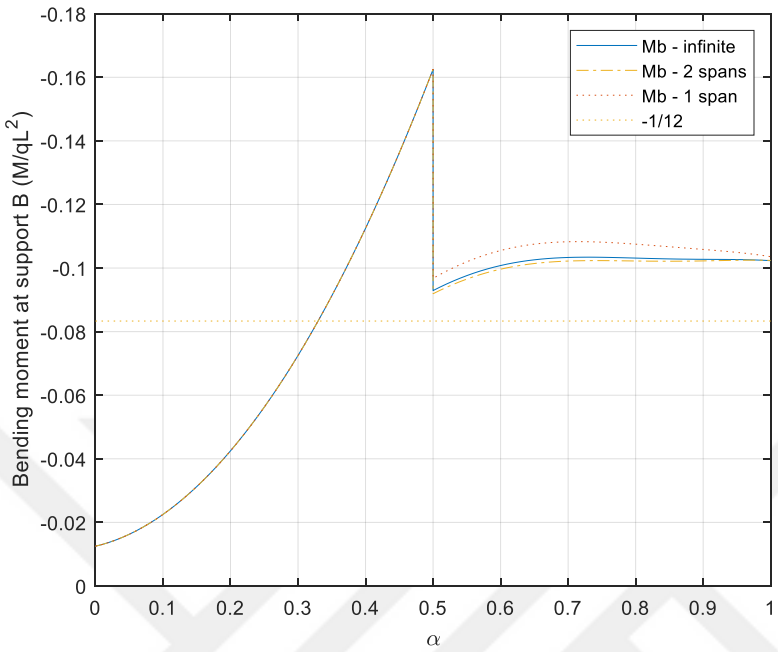

Figure 4.7. Bending Moment at Support B (α_L =0.5 α_q =0.1 α_{EI} =0.2)

Table 4.2 Percent Differences of M_B for normal launching nose

Compared Models	α					Max
	0	0.25	0.5	0.75	1	Moment
2 spans – Advanced	0.00%	0.00%	0.00%	-1.01%	0.08%	0.00%
1 span – Advanced	0.00%	0.00%	0.00%	4.60%	1.22%	0.00%

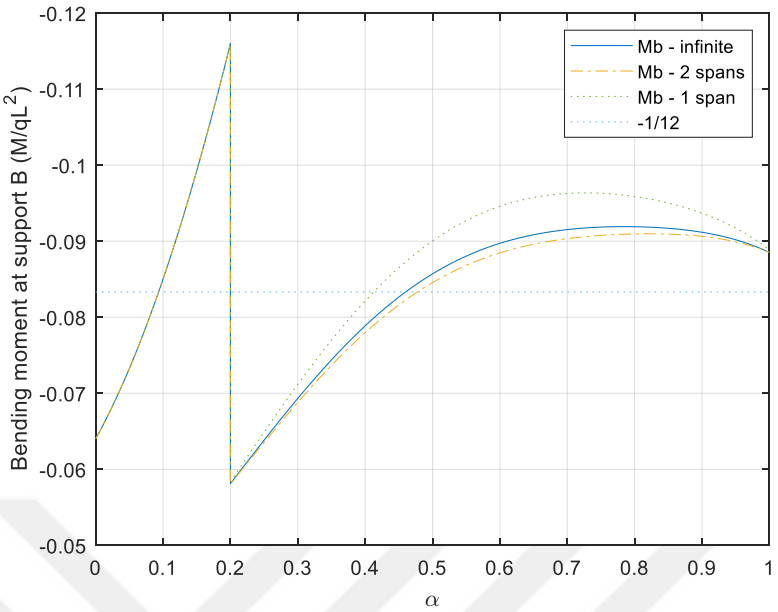

Figure 4.8. Bending Moment at Support B (α_L =0.8 α_q =0.2 α_{EI} =0.4)

Table 4.3 Percent Differences of M_B for long launching nose

Compared Models	α					Max
	0	0.25	0.5	0.75	1	Moment
2 spans – Advanced	0.00%	-0.41%	-1.33%	-1.19%	0.03%	0.00%
1 span – Advanced	0.00%	1.43%	4.99%	4.84%	0.39%	0.00%

Table 4.4, Table 4.5, and Table 4.6 show the percent difference of negative bending moment on support C on initial stage models (1 span and 2 spans) against the advanced stage model. 2 spans initial stage model generally has 5-7% higher moments during the launch. But maximum M_C generally occurs at the start of the launch, and 2 spans initial stage model has 5-7% lower value at the start of the launch.

1 span initial stage model has 5% to 36% lower moments during the launch. But its initial moment value is 18% (α_L =0.3) to 23% (α_L =0.8) higher than the advance stage. Differences for the maximum moment is 18% (α_L =0.3) to 21% (α_L =0.8). This big difference may cause critical problems, especially for the longer and lower stiffness launching noses where the moment on support C is higher than the support B. In that case, if only the advanced stage is considered, then moment calculation might result in a %20 lower than the actual value that occurred on the initial stage.

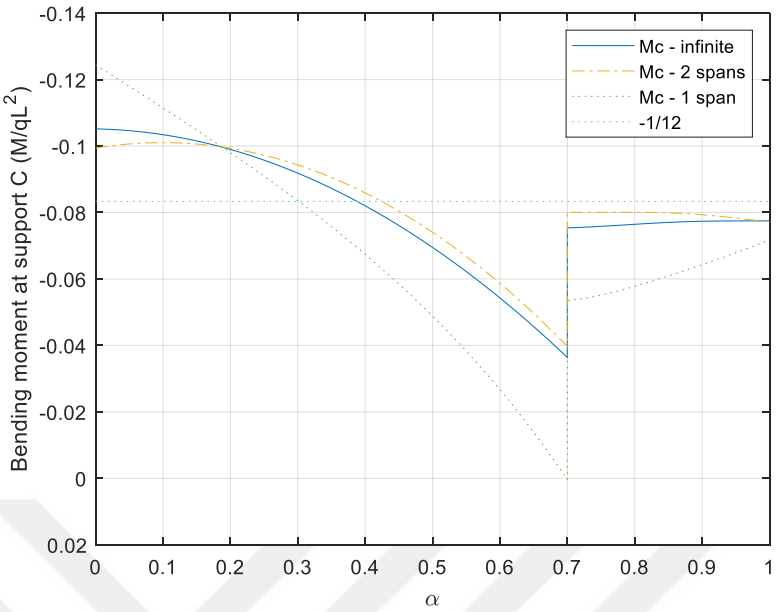

Figure 4.9. Bending Moment at Support C (α_L =0.3 α_q =0.05 α_{EI} =0.1)

Table 4.4 Percent Differences of M_C for short launching nose

Compared Models	α					Max
	0	0.25	0.5	0.75	1	Moment
2 spans – Advanced	-5.48%	1.57%	6.55%	5.58%	-0.50%	-3.94%
1 span – Advanced	18.33%	-5.04%	-29.73%	-27.27%	-7.40%	18.33%

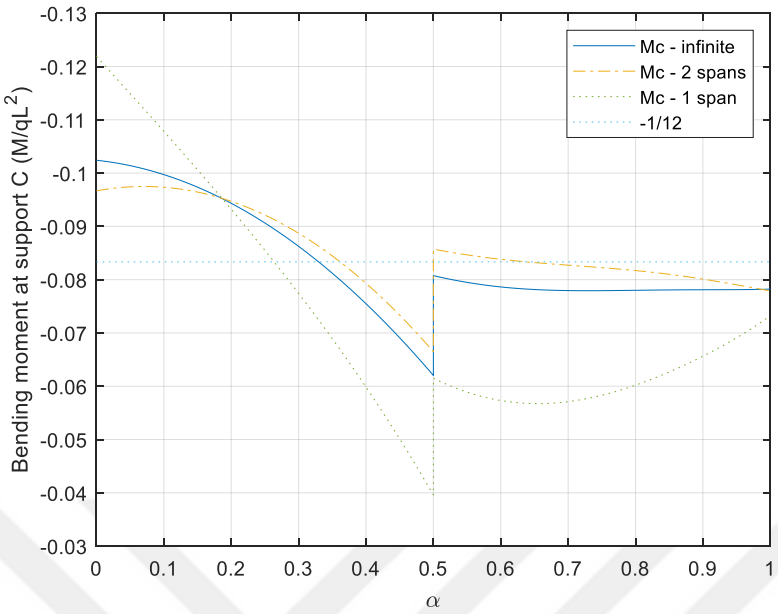

Figure 4.10. Bending Moment at Support C (α_L =0.5 α_q =0.1 α_{EI} =0.2)

Table 4.5 Percent Differences of M_C for long launching nose

Compared Models	α					Max
	0	0.25	0.5	0.75	1	Moment
2 spans – Advanced	-5.60%	1.66%	7.19%	5.54%	-0.43%	-4.80%
1 span – Advanced	19.01%	-5.67%	-36.18%	-25.19%	-6.40%	19.01%

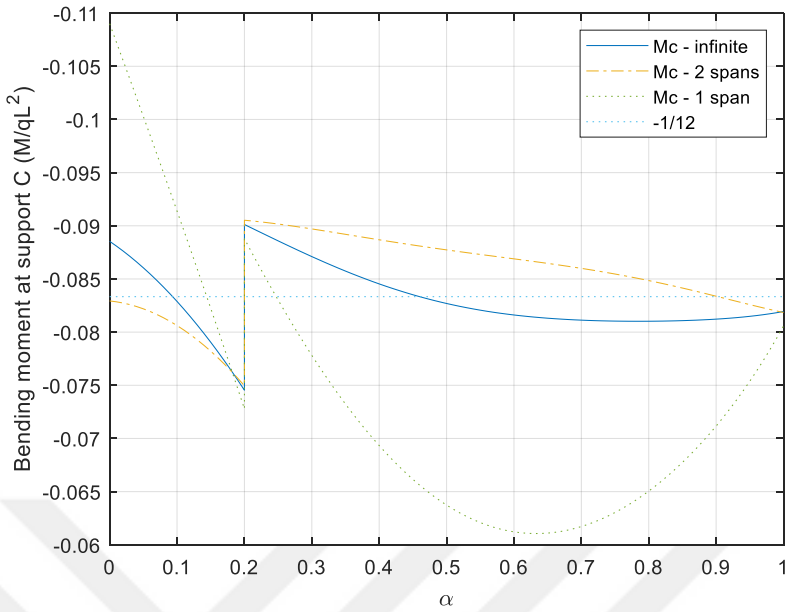

Figure 4.11. Bending Moment at Support C (α_L =0.8 α_q =0.2 α_{EI} =0.4)

Table 4.6 Percent Differences of M_C for long launching nose

Compared Models	α					Max
	0	0.25	0.5	0.75	1	Moment
2 spans – Advanced	-6.33%	1.53%	6.01%	5.46%	-0.11%	0.45%
1 span – Advanced	23.11%	-5.35%	-22.55%	-22.21%	-1.67%	20.95%

Table 4.7, Table 4.8, and Table 4.9 show the comparison of shear force acting on the support B on the initial stage models (with 1 and 2 spans launched) against the advanced stage model for 3 different types of launching noses. 2 spans initial stage model shows almost the same maximum shear forces with the advanced stage model with 0.2-0.5% differences. Even though the 1 span initial stage model shows slightly higher results (2-2.5%) than the advanced stage model, the difference is relatively small.

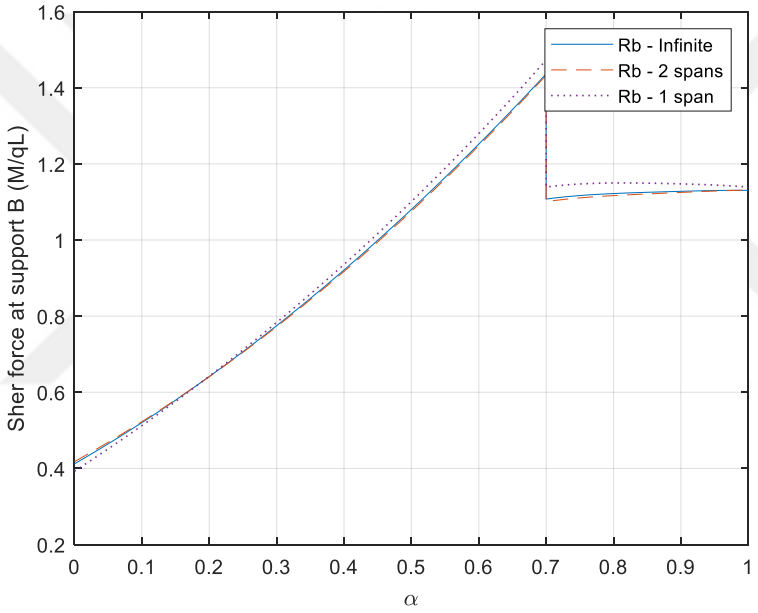

Figure 4.12. Shear Force at Support B (α_L =0.3 α_q =0.05 α_{EI} =0.1)

Table 4.7 Percent Differences of R_B for short launching nose Force

Compared Models	α					Max
	0	0.25	0.5	0.75	1	Force
2 spans – Advanced	1.40%	-0.21%	-0.42%	-0.56%	0.05%	-0.23%
1 span - Advanced	-4.68%	0.68%	1.91%	2.72%	0.76%	2.56%

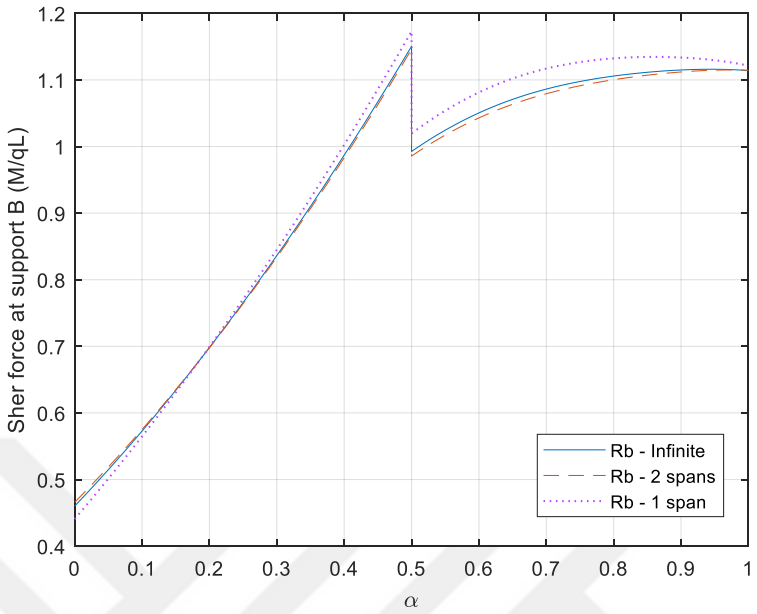

Figure 4.13. Shear Force at Support B (α_L =0.5 α_q =0.1 α_{EI} =0.2)

Table 4.8 Percent Differences of R_B for normal launching nose Force

Compared Models	α					Max
	0	0.25	0.5	0.75	1	Force
2 spans – Advanced	1.25%	-0.20%	-0.39%	-0.58%	0.05%	-0.39%
1 span - Advanced	-4.23%	0.67%	1.95%	2.66%	0.67%	1.95%

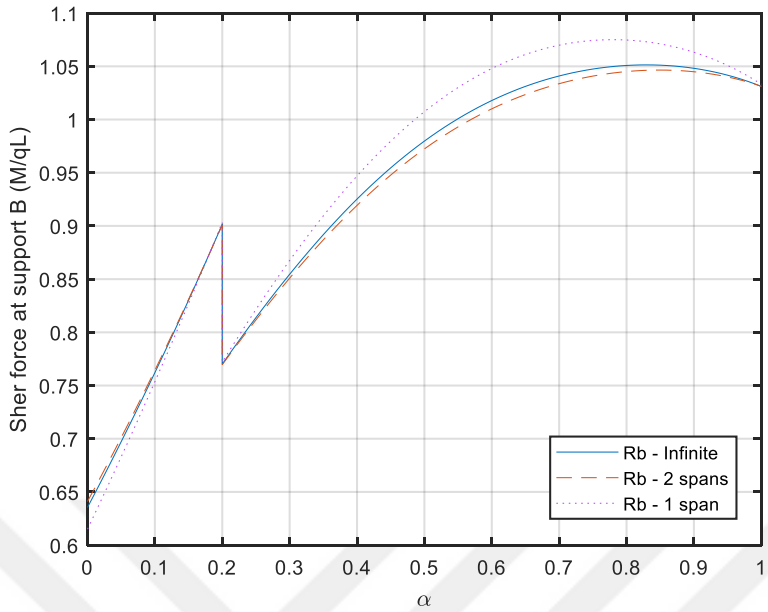

Figure 4.14. Shear Force at Support B (α_L =0.8 α_q =0.2 α_{EI} =0.4)

Table 4.9 Percent Differences of R_B for long launching nose Force

Compared Models	α					Max
	0	0.25	0.5	0.75	1	Force
2 spans – Advanced	0.88%	-0.23%	-0.74%	-0.63%	0.01%	-0.46%
1 span - Advanced	-3.22%	0.81%	2.79%	2.57%	0.20%	2.25%

Table 4.10, Table 4.11, and Table 4.12 show the comparison of tip deflection on the initial stages model (with 1 and 2 spans launched) against the advanced stage model for 3 different types of launching nose. Tip deflection values change during the launching, but the most critical deflection occurs at the end of phase 1 when the launching nose reached the target pier. After this maximum deflection, it hoisted with hydraulic equipment. This maximum deflection is taken into account for the comparisons between models.

The initial stage (1 span) model shows 6% less deflection than the advanced stage model for short and normal launching noses. For the longer launching nose difference is negligible (0.5%). The initial stage (2 spans) model shows almost the same deflection as the infinite model. The maximum difference is %1.35 for the maximum deflection. It can be said that the initial stages deflection is not significantly different than the advanced stage.

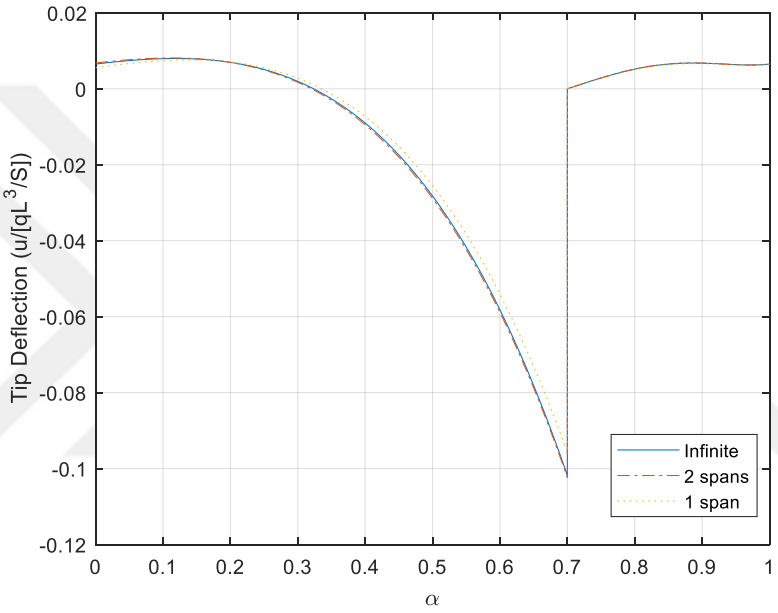

Figure 4.15. Tip Deflection of the Launching Nose (α_L =0.3 α_q =0.05 α_{EI} =0.1)

Table 4.10 Percent Differences of Tip Deflection for short launching nose

Compared Models	α					Max
	0	0.25	0.5	0.75	1	Deflection
2 spans – Advanced	4.43%	-2.71%	2.15%	0.70%	-0.07%	0.54%
1 span – Advanced	-14.80%	8.70%	-9.75%	-3.41%	-1.10%	-6.02%

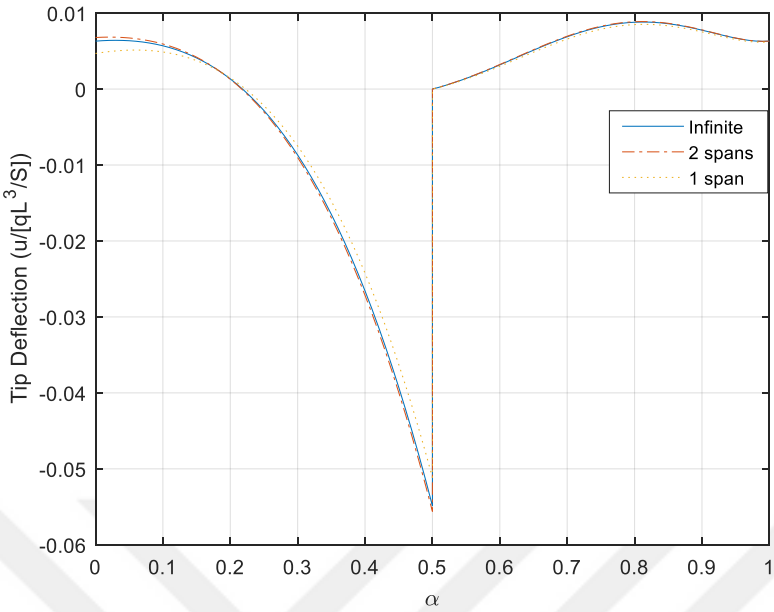

Figure 4.16. Tip Deflection of the Launching Nose (α_L =0.5 α_q =0.1 α_{EI} =0.2)

Table 4.11 Percent Differences of Tip Deflection for normal launching nose

Compared Models	α					Max
	0	0.25	0.5	0.75	1	Deflection
2 spans – Advanced	7.58%	6.63%	1.35%	0.86%	-0.11%	1.35%
1 span – Advanced	-25.71%	-22.66%	-6.82%	-3.93%	-1.65%	-6.82%

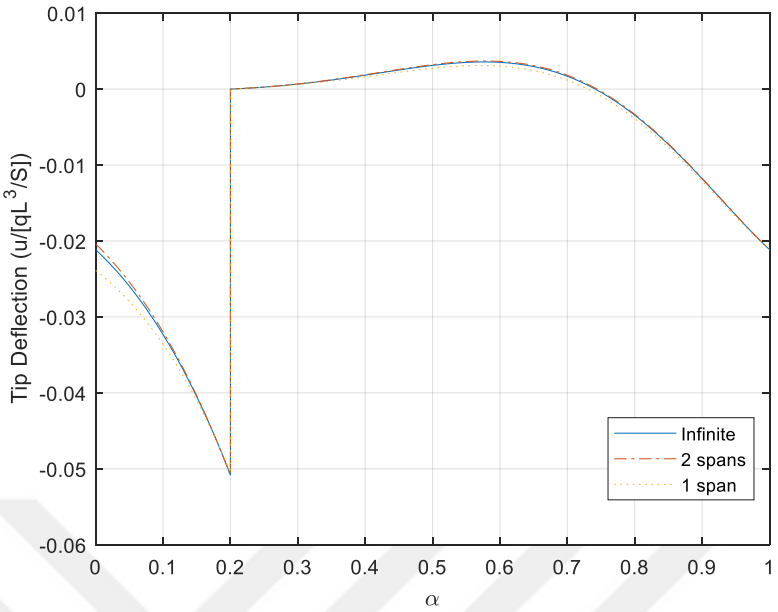

Figure 4.17. Tip Deflection of the Launching Nose (α_L =0.8 α_q =0.2 α_{EI} =0.4)

Table 4.12 Percent Differences of Tip Deflection for long launching nose

Compared Models	α					Max
	0	0.25	0.5	0.75	1	Deflection
2 spans – Advanced	-3.54%	1.97%	3.23%	-28.93%	0.01%	0.14%
1 span – Advanced	12.91%	-6.90%	-12.11%	117.62%	0.22%	-0.58%

4.3 Deflection of the Cantilever Deck and Launching Nose

Launching noses have two main contributions to the bridge during launching: decrease of the moment occurs due to cantilever span and decrease of deflection of cantilever span. Recovering from very high deflections would be problematic.

Therefore, the deflection should be limited to a chosen maximum value. Rosignoli (2014) mentions that 0.1 – 0.2m deflection might occur on prestressed concrete bridges and 1m or more deflection in steel girder bridges.

There are some studies that report the deflection occurs during the construction. Reno Bridge, a post-tensioned bridge, had 0.1m deflection (Ferretti, 2016). Paraná River Bridge is a steel bridge with a 100m span reached 0.93m deflection (Malite, Takeya, Gonçalves, & De Sáles, 2000); Wupper river valley bridge (72m span) is a composite bridge with 1.3m deflection (Marzahn, Hamme, Prehn, & Swadlo, 2007). San Cristobal bridge is also a composite bridge and had 1.05m deflection with a 180m span (Nader et al., 2007). Vaux bridge is a composite bridge with a very large span length of 130m, and maximum deflection during the launch reached 4.5m (Navarro et al., 2000).

Deflections should be carefully monitored during the launch. Nader et al. (2007) stated that during the San Cristobal bridge's launching, minor cracks occurred on the bridge and caused the decrease of the inertia. Consequently, this leads to an increase in the deflections. This logic may also apply backwardly. If the deflections during the launching are larger than the analysis results, unexpected cracks might have occurred on the bridge. It would be wise to check for cracks on the bridge in that situation.

In this chapter, the effects of launching nose design parameters (relative length, unit weight, and stiffness) on deflection were inspected. The previous chapter shows that advanced and initial stage deflection behaviors are not significantly different from each other. In this chapter advanced stage model with 3 spans launched is used for the comparison.

Figure 4.18 shows the relative launching nose length effects on the tip deflection for the chosen fixed relative unit weight and stiffness (α_q =0.1 α_{EI} =0.2). Shorter noses cause significantly higher deflections. Figure 4.19 shows the maximum deflection for each relative length. When the relative nose length decreases from 0.8 to 0.4, maximum deflection increased more than 2 times. A parabolic relation exists between tip deflection and relative launching nose lengths. Very short noses might cause unexpectedly large deflections.

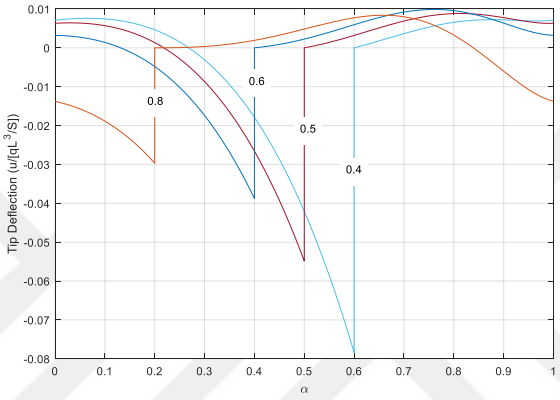

Figure 4.18. Tip Deflection of the Launching Nose changes with respect to different relative lengths (α_q =0.1 α_{EI} =0.2)

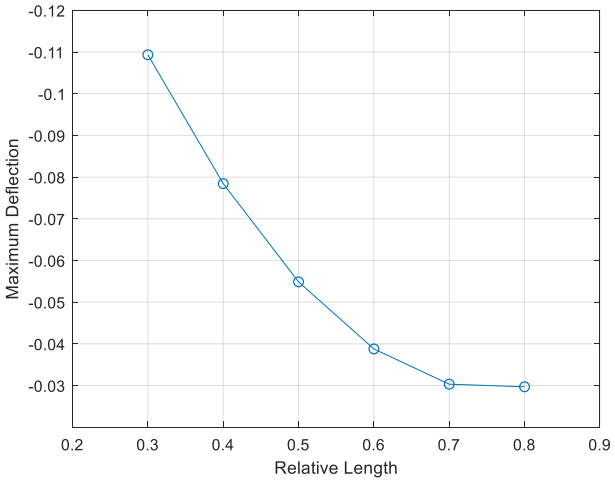

Figure 4.19. Maximum Tip Deflection of the Launching Nose with respect to different relative lengths (α_q =0.1 α_{EI} =0.2)

Figure 4.20 shows the effects of relative unit weights of the launching nose to the tip deflection for the chosen fixed relative length and stiffness (α_L =0.5 α_{EI} =0.2). As expected, heavier noses cause significantly higher deflections. Figure 4.21 shows the maximum deflection for different relative unit weights. A linear relationship between maximum deflection and relative unit weight can be easily observed.

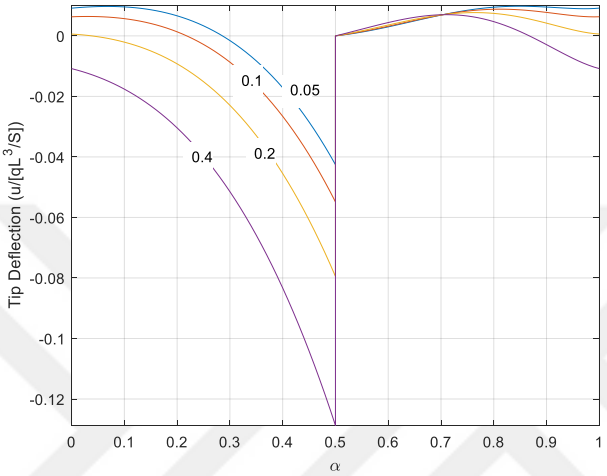

Figure 4.20. Tip Deflection of the Launching Nose changes with respect to different relative unit weight (α_L =0.5 α_{EI} =0.2)

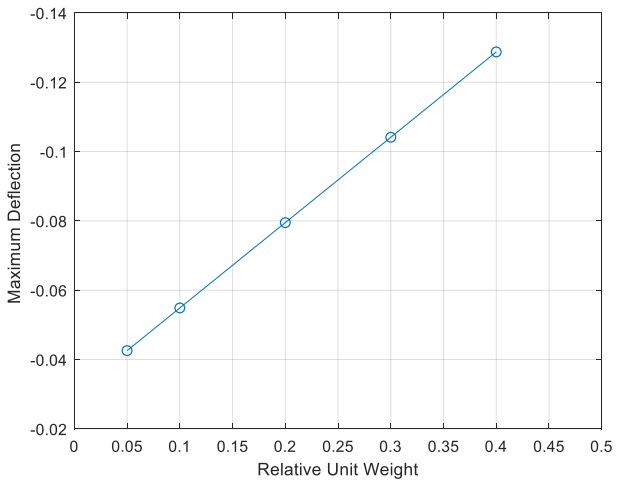

Figure 4.21. Maximum Tip Deflection of the Launching Nose with respect to different relative bending stiffnesses (α_L =0.5 α_{EI} =0.2)

Figure 4.22 shows the effects of relative unit weights of the launching nose to the tip deflection for the chosen fixed relative length and unit weights (α_L =0.5 α_q =0.1). Launching noses with lower stiffness values cause higher deflections. Figure 4.23 shows the maximum deflection for different relative stiffnesses. Stiffness changes on lower stiffness values are much more effective than the changes on higher stiffness values. When the required stiffness is satisfied, it is not cost-effective to increase further. This behavior is similar to stiffness's effect on bending moment on support B, where increasing stiffness excessively did not decrease the maximum moment.

For these comparisons, it can be concluded that all three parameters are effective on the maximum cantilever deflection. The most important parameter is the relative launching nose length. For the case of excessive deflections, the first solution might be increasing the relative nose length.

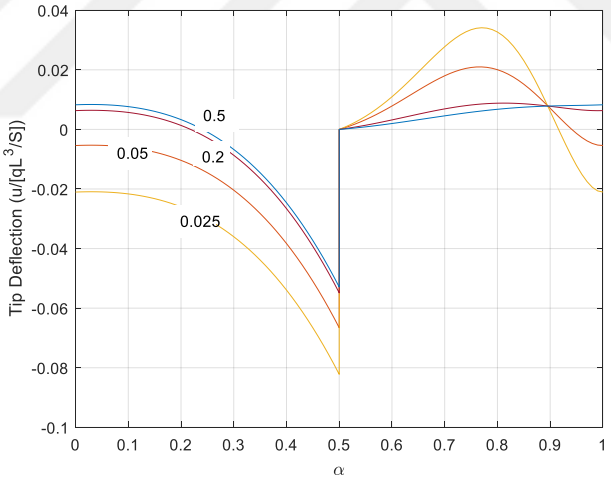

Figure 4.22. Tip Deflection of the Launching Nose changes with respect to different relative stiffnesses (α_L =0.5 α_q =0.1)

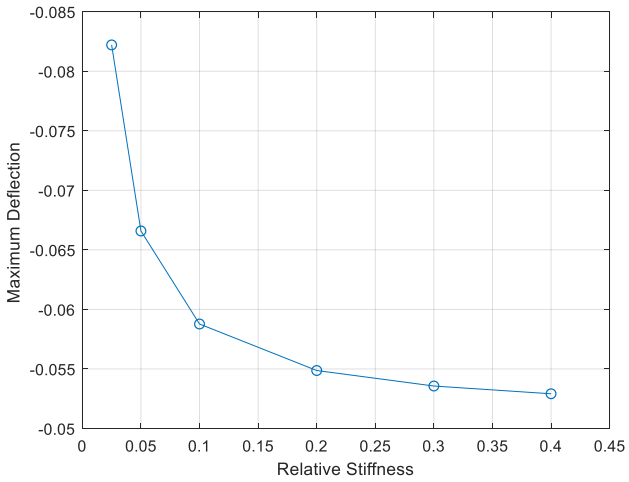

Figure 4.23. Maximum Tip Deflection of the Launching Nose with respect to different relative stiffnesses (α_L =0.5 α_q =0.1)

Following real-life cross-section data based on Yalın (2019) will be used to present the deflection of the launching nose and the effects of parameters more clearly.

- Unit Weight=25 kN/m^3
- A=13.73 m^2
- I=22.75 m^4
- E=36 GPa
- L=60m

Following 3 sets of launching nose parameters will be used.

- α_L =0.3 α_q =0.05 α_{EI} =0.1 – Shorter, lighter and lower stiffness launching nose
- α_L =0.5 α_q =0.1 α_{EI} =0.2 – Normal launching nose
- α_L =0.8 α_q =0.2 α_{EI} =0.4 – Longer, heavier and higher stiffness launching nose

Figure 4.24 shows the deflection of the cantilever launching nose for 3 different kinds of launching nose. Maximum deflection changes from 0.27cm to 0.55cm. A

very short launching nose causes high deflections, and longer launching noses cause lower deflection values. Increasing the length of the launching nose decrease the deflection but a longer launching also requires higher unit weight (Equations (3.23) and (3.24)). Therefore, decreasing deflections beyond a certain point is harder.

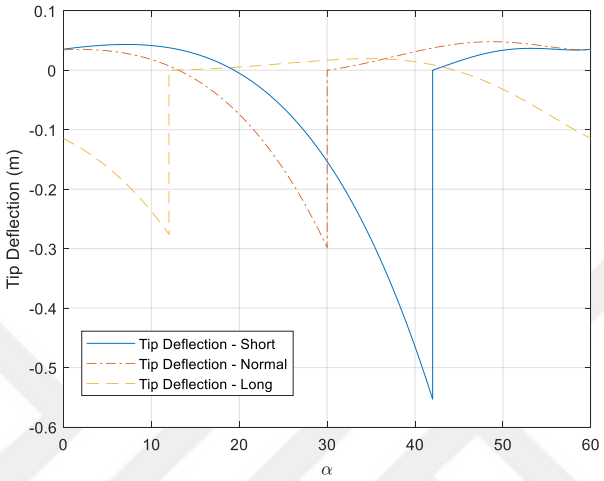

Figure 4.24. Tip Deflection of the Launching Nose for realistic example with different launching nose types

Figure 4.25 shows the relation between cantilever deflection and the negative bending moment on support B during phase 1 for 3 types of launching noses. It can be seen that there is an almost linear relationship between the negative moment and deflection during the launch.

Figure 4.26 shows the relation between cantilever deflection and the shear force on support B. A similar correlation can also be observed between shear force and cantilever deflection, both increase during phase 1.

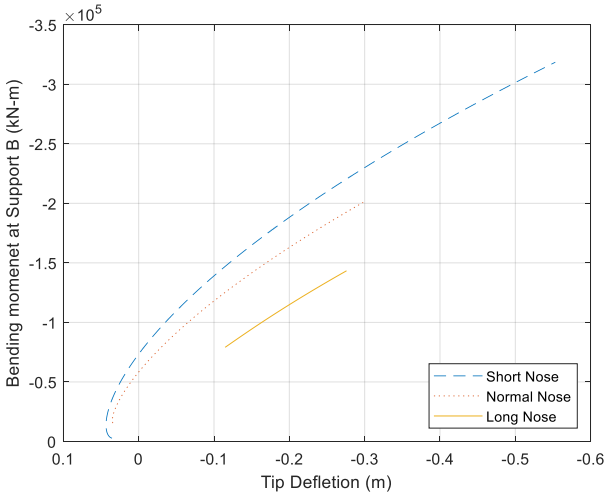

Figure 4.25. Bending moment at support B with respect to Tip Deflection with different launching nose types

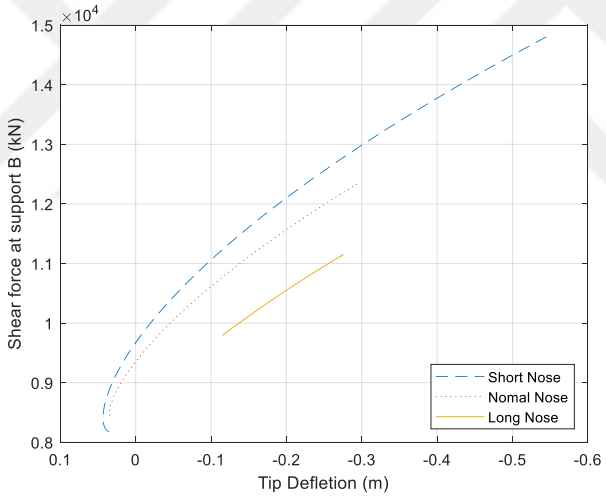

Figure 4.26. Shear force at support B with respect to Tip Deflection with different launching nose types

It is mentioned that very high tip deflections might cause problems. When the nose is reached the next pier, hydraulic equipment is used to realign the launching nose to the bearing level. An uplift force is applied to the launching nose by hydraulic equipment to lift it. This force is limited by the equipment's capacity; therefore, the nose should be designed with this consideration. Figure 4.27 shows the change of

the required uplift force against the maximum deflection for different kinds of launching noses. It shows that launching noses with high deflections also requires higher uplift forces.

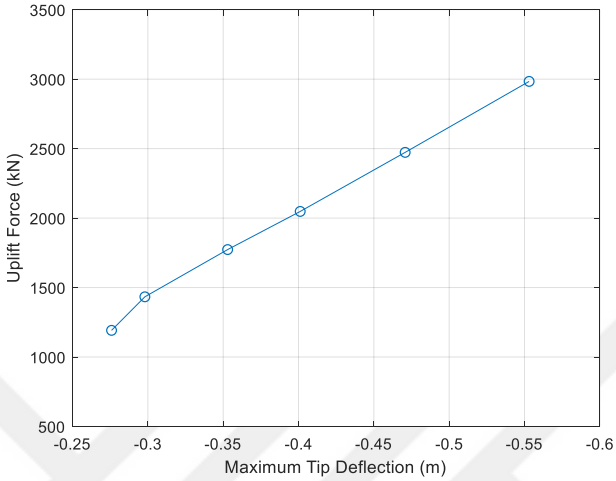

Figure 4.27. Maximum Tip Deflection vs. Uplift Force for different launching nose types

CHAPTER 5

SUMMARY AND CONCLUSIONS

5.1 Summary

The current launching nose optimization methods in the literature only consider the advanced stage of the launching. Therefore, in this thesis, a finite element model for the initial stage analysis has been developed in MATLAB to investigate the initial stage of the construction. This initial stage model also has new features such as deflection check and the movement of the newly casted section at the yard. Both were not considered in the current advanced stage models.

In current advanced stage methods, the rearward joint is modeled as a fixed joint. However, in reality, there is no restriction against the rotation on the yard. Therefore, this part is modeled as a pin joint in the initial stage model. The newly casted section at the yard will move during the launch; consequently, the rearward joint will also move. Therefore, the newly casted section is modeled with dynamic dimensions during the launching. Current methods do not consider the deflection of the cantilever deck section and launching nose. However, excessive deflections may occur during the launching, especially at the end of phase 1, just before the launching nose tip reach the target pier. Thus, the cantilever launching nose is also modeled in the new model to have the deflection results.

Advanced stage models use a theoretical dimensionless model; this same model is also used in the initial stage model. It is assumed that all the span sizes are the same without any curvature; the launching nose and deck girder crosssections are constant through the length. Only dead load is applied on the system during the launching. Loads due to the wind and seismic effects are not considered. It is also assumed neoprene plates between the girder and the piers will decrease the friction between

the girder and the piers. Therefore, effects due to friction are neglected. Shear, temperature, and settlement effects are also not considered in the design.

The initial stage models with 1 and 2 launched spans are compared against the advanced stage model to understand differences between the initial stage and advanced stage behaviors. 3 different sets of launching nose parameters (short, normal, and long) are chosen for this comparison. Normal launching parameters (α_L=0.5 α_q=0.1 α_{EI}=0.2) are chosen based on the popular models in the literature. Short and long nose parameters are derived from the normal launching nose.

Three main parameters' effects on the deck moments have been studied in the literature, but their effects on the deflection have not been studied because current models do not check the cantilever deflection. Therefore, the change of the deflection based on main design parameters (relative length, unit weight, and stiffness) is studied in this thesis. Deflection changes on a realistic model are also explained.

5.2 Conclusion

Following conclusions has been reached in the analysis and the comparisons in this thesis:

- Maximum moments on support B (launching support) are the same for the semi-infinite beam models and infinite beam model but the maximum moment on support C (one support behind the launching support) are different on each model. The semi-infinite beam model with 2 spans shows slightly higher moment results on the support C than the infinite beam model; however semi-infinite beam model with the 3 spans almost shows the same behavior as the infinite beam model. Thus, the semi-infinite beam model can be used for representing advanced construction stages.
- The numerical optimization method is the most comprehensive optimization method for the preliminary launching nose design. This method checks the maximum moment conditions on several supports and span points and also

includes restrictions regarding the relative length and unit weight relationship.

- Following results have been reached in the comparison of the initial stage and advanced stage models.
    - Maximum moment values on support B are the same for all methods.
    - Initial stage models' maximum cantilever deflection and maximum shear force on support B are not significantly different from the advanced stage models.
    - The maximum negative moment on support C is around 20% higher on the initial stage model than the advanced stage model. This case might especially be critical for the long launching noses where the maximum critical moment occurs on C rather than B. Therefore, the initial stage launching should also be checked in case of maximum moments occurrence on support C.
- It is found that all three main launching nose parameters are effective on the maximum deflection. Relative length is the most effective parameter on the maximum deflection. Launching noses with α_L lower than 0.6 will be subjected to excessive deflections. Relative unit weight is the second important parameter on the deflection. Launching noses heavier than α_q=0.2 might cause undesirable deflections. Relative stiffness is the least effective parameter; it only slightly affects the maximum deflection. The launching nose should have an α_L value higher than 0.6 and α_q value lower than 0.2 to have reasonably low cantilever deflection.
- It is observed that the moment and shear effects on the last launched support have a direct relationship with the deflection during the launch. Also required uplift force to realign the launching nose to the bearing level is related to the maximum deflection of the launching nose.

Recommendations for future research:

- Current optimization methods only consider the advanced stage of the launching, and they do not check the deflection of the cantilever launching nose. These optimization methods can be improved further to analyze both the initial and advanced stages while considering deflection.
- Currently, it is assumed that launching nose unit weight and stiffness are constant through the length, but in practice, launching noses of the post-tensioned concrete box bridges are generally made of tapered I beams that have varying weight and stiffness. These tapered noses can be modeled accurately with finite element methods. Then, these models can be compared with the linear noses to test the current linear nose assumption's accuracy.
- The current methods assume that span lengths are equal and bridge geometry is linear; however, this may not correct all bridges. Span lengths can be different, especially on the first and last spans of the bridge. This change's effects on the launching moments should be studied. Also, a bridge may have curvature; in that case, the effects of the torsional moments and uneven shear effects on the design are required to be studied.
- Launching noses have three main parameters: relative length, unit weight, and stiffness. Constraints between the launching nose's unit weight and length are provided by Rosignoli (1998). However, the relation between stiffness and other parameters is unknown; without these relationship constraints, optimization studies may result in unrealistic nose designs. The relationship between stiffness and other parameters should be studied to have better optimization methods.
- Shear related deflections are not considered in the current methods. Effects of shear related internal forces and deflections on the incremental launching bridges can be further studied.
- The only external load acting on the system is the dead load of the bridge deck and the launching nose in the current models. However, wind and seismic effects might also occur during the launching and effects the design. Their effects on the launch nose can be studied.

- Friction between bearings and girder does not take into account in the current methods. The occurrence of the extra moment on the deck section due to this friction also required to be studied.

REFERENCES

Arici, M., & Granata, M. F. (2007). Analysis of curved incrementally launched box concrete bridges using the Transfer Matrix Method. *Bridge Structures*, *3*(3–4), 165–181. https://doi.org/10.1080/15732480701510445

Bennett, M. V., & Taylor, A. J. (2002). Woronora River Bridge, Sydney. *Structural Engineering International*, *12*(1), 28–31. https://doi.org/10.2749/101686602777965766

Buonomo, M., Servant, C., Virlogeux, M., Cremer, J.-M., Goyet, V. de V. de, & Forno, J.-Y. Del. (2004). The design and the construction of the Millau Viaduct. *Steelbridge 2004*, (October 2001), 165–182.

Burkitt, S., Team, D., Structures, L., & Alliance, C. H. C. (2009). Design of Two Incrementally Launched Bridges on the Coopernook to Herons Creek Section of the Pacific Highway. *Austroads Bridge Conference, 7th, 2009, Auckland, New Zealand*, (February), 1–17.

Chacón, R., Uribe, N., & Oller, S. (2016). Numerical Validation of the Incremental Launching Method of a Steel Bridge Through a Small-Scale Experimental Study. *Experimental Techniques*, *40*(1), 333–346. https://doi.org/10.1007/s40799-016-0037-5

Chacón, R., & Zorrilla, R. (2015). Structural Health Monitoring in Incrementally Launched Steel Bridges: Patch Loading Phenomena Modeling. *Automation in Construction*, *58*, 60–73. https://doi.org/10.1016/j.autcon.2015.07.001

De Clercq, E., & De Ridder, J. (2003). Curved Bridge Mechelse Steenweg, Kortenberg, Belgium. *Structural Engineering International*, *13*(1), 14–16. https://doi.org/10.2749/101686603777964991

Favre, R., Badoux, M., Burdet, O., & Laurencet, P. (1999). Design of a curved incrementally launched bridge. *Structural Engineering International: Journal of the International Association for Bridge and Structural Engineering (IABSE)*, *9*(2), 128–132. https://doi.org/10.2749/101686699780621064

Ferretti, T. L. (2016). Case study. In *Innovative Bridge Design Handbook* (pp. 639–669). https://doi.org/10.1016/B978-0-12-800058-8.00024-4

Fontan, A. N., Diaz, J. M., Baldomir, A., & Hernandez, S. (2010). Improved Optimization Formulations for Launching Nose of Incrementally Launched Prestressed Concrete Bridges. *Journal of Bridge Engineering*, *16*(3), 461–470. https://doi.org/10.1061/(asce)be.1943-5592.0000169

Fontán, A. N., Hernández, S., & Baldomir, A. (2013). Simultaneous Cross Section and Launching Nose Optimization of Incrementally Launched Bridges. *Journal of Bridge Engineering*, *19*(3), 04013002. https://doi.org/10.1061/(asce)be.1943-5592.0000523

Furlanetto, G., Torricelli, L. F., & Marchiondelli, A. (2010). Launching of the Reno Bridge on the A1 highway, Italy. *Structural Engineering International:*

Journal of the International Association for Bridge and Structural Engineering (IABSE), *20*(1), 26–30. https://doi.org/10.2749/101686610791555676

Göhler, B., & Pearson, B. (2000). *Incrementally Launched Bridges: Design and Construction* (1st ed.). Wiley VCH, 2000.

Granata, M. F. (2014). Analysis of non-uniform torsion in curved incrementally launched bridges. *Engineering Structures*, *75*, 374–387. https://doi.org/10.1016/j.engstruct.2014.05.047

Granata, M. F. (2015). Adjustable prestressing for construction stages of incrementally launched bridges. *European Journal of Environmental and Civil Engineering*, *19*(3), 327–346. https://doi.org/10.1080/19648189.2014.949871

Granath, P. (1998). Distribution of support reaction against a steel girder on a launching shoe. *Journal of Constructional Steel Research*, *47*(3), 245–270. https://doi.org/10.1016/S0143-974X(98)00006-6

Granath, P. (2000). Serviceability limit state of I-shaped steel girders subjected to patch loading. *Journal of Constructional Steel Research*, *54*(3), 387–408. https://doi.org/10.1016/S0143-974X(99)00057-7

Granath, P., Thorsson, A., & Edlund, B. (2000). I-shaped steel girders subjected to bending moment and travelling patch loading. *Journal of Constructional Steel Research*, *54*(3), 409–421. https://doi.org/10.1016/S0143-974X(99)00071-1

Hernandez, S., & Fontan, A. N. (2014). Cost optimization in bridge construction: Application to launched bridges. *Structures Congress 2014 - Proceedings of the 2014 Structures Congress*, 2801–2812. https://doi.org/10.1061/9780784413357.245

Hirmand, M. R., Moghadam, A., & Riahi, H. T. (2013). A Mathematical Investigation on the Optimum Design of the Nose-Deck System in Incrementally Launched Bridges. *European Journal of Scientific Research*, *108*(1), 38–52.

Hu, Z., Wu, D., & Sun, L. Z. (2015). Integrated investigation of an incremental launching method for the construction of long-span bridges. *Journal of Constructional Steel Research*, *112*, 130–137. https://doi.org/10.1016/j.jcsr.2015.05.001

Jung, K., Kim, K., Sim, C., & Kim, J. J. (2011). Verification of incremental launching construction safety for the Ilsun Bridge, the world's longest and widest prestressed concrete box girder with corrugated steel web section. *Journal of Bridge Engineering*, *16*(3), 453–460. https://doi.org/10.1061/(ASCE)BE.1943-5592.0000165

Laviolette, M. (HNTB C., Wipf, T., Lee, Y., Bigelow, J., & Phares, B. (2007). *Bridge Construction Practices Using Incremental Launching*.

Liddle, R. (2010). The launching of the River Esk bridge, UK. *Proceedings of the Institution of Civil Engineers - Bridge Engineering*, *163*(3), 137–146.

https://doi.org/10.1680/bren.2010.163.3.137

Lontai, A., Nagy, A., & Mihalek, T. (2008). Viaducts Built Using Incremental Launching Method on the M7 Motorway in Hungary Incremental Launching. *Concrete Structures*, 23–26.

Lopez, L. M.-T. (2010). Guareña Viaduct. Retrieved January 10, 2021, from https://structurae.net/en/media/251198-guarena-viaduct

Malite, M., Takeya, T., Gonçalves, R. M., & De Sáles, J. J. (2000). Monitoring of the Paraná River Bridge during launching. *Structural Engineering International: Journal of the International Association for Bridge and Structural Engineering (IABSE)*, *10*(3), 193–196. https://doi.org/10.2749/101686600780481464

Marchetti, M. E. (1984). Specific design problems related to bridges built using the incremental launching method. *Engineering Structures*, *6*(3), 185–210. https://doi.org/10.1016/0141-0296(84)90046-4

Marzahn, G. A., Hamme, M., Prehn, W., & Swadlo, J. (2007). Wupper river valley bridge: A state-of-the-art composite bridge. *Structural Engineering International: Journal of the International Association for Bridge and Structural Engineering (IABSE)*, *17*(1), 35–39. https://doi.org/10.2749/101686607779938822

Nader, M., Manzanarez, R., Lopez-Jara, J., & De La Mora, C. (2007). Launching of the San Cristobal Bridge. *Transportation Research Record: Journal of the Transportation Research Board*, *2040*(1), 57–68. https://doi.org/10.3141/2040-07

Navarro, M. G., Lebet, J.-P., & Beylounü, R. (2000). Launching of the Vaux Viaduct. *Structural Engineering International*, *10*(1), 16–18. https://doi.org/10.2749/101686600780621017

Özel, C. N., Kutsal, K., & Özkul, Ö. (2019). Eğim Aşağı Yönde İtme-Sürme Çayırköy Viyadüğü. *4. Köprüler ve Viyadükler Sempozyumu*, 355–363. Ankara: TMMOB İnşaat Mühendisleri Odası Ankara Şubesi.

Popov, O. A., & Seliverstov, V. A. (1998). Steel Bridges on Ankara's Peripheral Motorway. *Structural Engineering International*, *8*(3), 205–210. https://doi.org/10.2749/101686698780489171

Ramakrishna, A., & Sankaralingam, C. (1997). Panval Nadhi Viaduct, India. *Structural Engineering International*, *7*(3), 168–170. https://doi.org/10.2749/101686697780494716

Rosignoli, M. (1997). Solution of the continuous beam in launched bridges. *Proceedings of the Institution of Civil Engineers: Structures and Buildings*, *122*(4), 390–398. https://doi.org/10.1680/istbu.1997.29828

Rosignoli, M. (1998). Nose-Deck Interaction in Launched Prestressed Concrete Bridges. *Journal of Bridge Engineering*, *3*(1), 21–27. https://doi.org/10.1061/(ASCE)1084-0702(1998)3:1(21)

Rosignoli, M. (1999). Prestressing Schemes for Incrementally Launched Bridges. *Journal of Bridge Engineering*, *4*(MAY), 107–115.

Rosignoli, M. (2000). Thrust and guide devices for launched bridges. *Journal of Bridge Engineering*, *5*(1), 75–83. https://doi.org/10.1061/(ASCE)1084-0702(2000)5:1(75)

Rosignoli, M. (2002). *Bridge Launching* (1st ed.). Thomas Telford Publishing.

Rosignoli, M. (2014). *Bridge Launching* (2nd ed.). https://doi.org/10.1680/bl.31463

Sasmal, S., & Ramanjaneyulu, K. (2006). Transfer matrix method for construction phase analysis of incrementally launched prestressed concrete bridges. *Engineering Structures*, *28*(13), 1897–1910. https://doi.org/10.1016/j.engstruct.2006.03.017

Sasmal, S., Ramanjaneyulu, K., Srinivas, V., & Gopalakrishnan, S. (2004). Simplified computational methodology for analysis and studies on behaviour of incrementally launched continuous bridges. *Structural Engineering and Mechanics*, *17*(2), 245–266. https://doi.org/10.12989/sem.2004.17.2.245

Shao, C. Y. (2013). The New Incremental Launching Construction Technology of Jiubao Bridge Long-span Hybrid Arch-girder Structure. *Journal of Civil Engineering and Science*, *2*(4), 250–254.

Shojaei, A., Tajmir Riahi, H., & Hirmand, M. (2015). Finite element modeling of incremental bridge launching and study on behavior of the bridge during construction stages. *International Journal of Civil Engineering*, *13*(1), 112–125. https://doi.org/http://dx.doi.org/10.22068/IJCE.13.1.112

Wang, W., Zheng, H., & Zeng, X. (2010). Optimum Design of Launching Nose during Incremental Launching Construction of Same-Span Continuos Bridge. *International Journal of Structural and Construction Engineering*, *4*(12), 420–425. https://doi.org/doi.org/10.5281/zenodo.1075298

Wu, X., Wu, T., & Chen, W. (2018). Analysis of height difference between three trusses of a steel truss bridge during incremental launching. *Stahlbau*, *87*(9), 910–922. https://doi.org/10.1002/stab.201810632

Xu, R., & Shao, B. (2012). New Beam Element for Incremental Launching of Bridges. *Journal of Bridge Engineering*, *17*(5), 822–826. https://doi.org/10.1061/(ASCE)BE.1943-5592.0000315

Yalın, M. (2019). *İtme Sürme Yöntemi ile Viyadük Yapımı*. İstanbul Teknik Üniversitesi.

Zellner, W., & Svensson, H. (1983). Incremental launching of structures. *Journal of Structural Engineering (United States)*, *109*(2), 520–537. https://doi.org/10.1061/(ASCE)0733-9445(1983)109:2(520)

APPENDICES

A. MATLAB Analysis Code

This chapter explains the structural analysis code developed in MATLAB for the initial construction stage analysis of the incremental launching method. The code structure is as follows:

a. phase1initialStage.m: finite element solution script of phase 1 of the launching

b. phase2initialStage.m: finite element solution script of phase 2 of the launching

c. createElement.m: function for creating element stiffness and load matrices

a. phase1initialStage.m

```
syms E I L q En In Ln qn S Sn Lx dum...
    V1 V2 V3 V4 V5 V6 M1 M2 M3 M4 M5 M6...
    d1 fi1 d2 fi2 d3 fi3 d4 fi4 d5 d6 fi5 fi6

numLaunchedSpan=1;
numMember=numLaunchedSpan+3;
numDof=numMember*2+2;
memberLenght=1;

%Creates element stiffness and FEM matrix

%Newly casted span at the yard
i=1;
element(i)=createElement(q,L-Lx,S,0,L-Lx);

%Already launched spans
for i=2:numMember-2
element(i)=createElement(q,L,S,element(i-1).coor(2),element(i-
1).coor(2)+memberLenght);
end

%Launching span
i=numMember-1;
```

```
element(i)=createElement(q,Lx,S,element(i-1).coor(2),element(i-
1).coor(2)+Lx);

%Launcing nose
i=numMember;
element(i)=createElement(qn,Ln,Sn,element(i-1).coor(2),element(i-
1).coor(2)+Ln);

% Create empty global stiffness and fixed end moment matrix
K(numDof,numDof)=dum;
FEM(numDof,1)=dum;

%Assemble global stiffness and FEM matrix
for i=1:numMember
k(i).stiffness(numDof,numDof)=dum;
k(i).stiffness(i*2-1:i*2+2,i*2-1:i*2+2)=element(i).stiffness;
K=K+k(i).stiffness;

fem(i).fixes(numDof,1)=dum;
fem(i).fixes(i*2-1:i*2+2)=element(i).FEM;
FEM=FEM+fem(i).fixes;
end

%Clear the dummy
dum=0;
K=subs(K);
FEM=subs(FEM);

%Assign constraints to the nodes
switch numMember
    case 4
        Ext=[V1;M1;V2;M2;V3;M3;V4;M4;V5;M5];
        fi=[d1;fi1;d2;fi2;d3;fi3;d4;fi4;d5;fi5];
        M1=0;
        M2=0;
        M3=0;
        M4=0;
        M5=0;
        d1=0;
        d2=0;
        d3=0;
        V4=0;
        V5=0;
        unk=[fi1;fi2;fi3;fi4;fi5;V1;V2;V3;d4;d5];
    case 5
        Ext=[V1;M1;V2;M2;V3;M3;V4;M4;V5;M5;V6;M6];
        fi=[d1;fi1;d2;fi2;d3;fi3;d4;fi4;d5;fi5;d6;fi6];
        M1=0;
        M2=0;
        M3=0;
        M4=0;
        M5=0;
        M6=0;
        d1=0;
```

```
        d2=0;
        d3=0;
        d4=0;
        V5=0;
        V6=0;
        unk=[fi1;fi2;fi3;fi4;fi5;fi6;V1;V2;V3;V4;d5;d6];
end

%Solve global stiffness equation
eqn=(Ext==K*fi+FEM);
solve(eqn);
sol=solve(eqn,unk);

%Assign results to each node
switch numMember
    case 4
     fi1=subs(sol.fi1);
     fi2=subs(sol.fi2);
     fi3=subs(sol.fi3);
     fi4=subs(sol.fi4);
     fi5=subs(sol.fi5);
     V1=subs(sol.V1);
     V2=subs(sol.V2);
     V3=subs(sol.V3);
     d4=subs(sol.d4);
     d5=subs(sol.d5);
    case 5
     fi1=subs(sol.fi1);
     fi2=subs(sol.fi2);
     fi3=subs(sol.fi3);
     fi4=subs(sol.fi4);
     fi5=subs(sol.fi5);
     fi6=subs(sol.fi6);
     V1=subs(sol.V1);
     V2=subs(sol.V2);
     V3=subs(sol.V3);
     V4=subs(sol.V4);
     d5=subs(sol.d5);
     d6=subs(sol.d6);
end

 %Solve element stiffness matrix equations
 for i=1:numMember
 element(i).deflection =fi(2*i-1:2*i+2);

element(i).forces=subs(element(i).stiffness*element(i).deflection+e
lement(i).FEM);
 end
```

b. phase2initialStage.m

```
syms E I L q En In Ln qn S Sn Lx dum...
    V1 V2 V3 V4 V5 V6 V7 M1 M2 M3 M4 M5 M6 M7...
    d1 fi1 d2 fi2 d3 fi3 d4 fi4 d5 d6 fi5 fi6 d7 fi7

%number of variables
numLaunchedSpan=1;
numMember=numLaunchedSpan+4;
numDof=numMember*2+2;
memberLenght=1;

%Creates element stiffness and FEM matrix

%Newly casted span at the yard
i=1;
element(i)=createElement(q,L-Lx,S,0,L-Lx);

%Already launched spans
for i=2:numMember-2
element(i)=createElement(q,L,S,element(i-1).coor(2),element(i-
1).coor(2)+memberLenght);
end

%Launching span
i=numMember-2;
element(i)=createElement(q,Lx,S,element(i-1).coor(2),element(i-
1).coor(2)+Lx);

%Launcing nose left side
i=numMember-1;
element(i)=createElement(qn,L-Lx,Sn,element(i-1).coor(2),element(i-
1).coor(2)+memberLenght-Lx);

%Launcing nose right side
i=numMember;
element(i)=createElement(qn,Ln-L+Lx,Sn,element(i-
1).coor(2),element(i-1).coor(2)+Ln+Lx-memberLenght);

% Create empty global stiffness and fixed end moment matrix
K(numDof,numDof)=dum;
FEM(numDof,1)=dum;

%Assemble global stiffness and FEM matrix
for i=1:numMember
k(i).stiffness(numDof,numDof)=dum;
k(i).stiffness(i*2-1:i*2+2,i*2-1:i*2+2)=element(i).stiffness;
K=K+k(i).stiffness;

fem(i).fixes(numDof,1)=dum;
fem(i).fixes(i*2-1:i*2+2)=element(i).FEM;
FEM=FEM+fem(i).fixes;
end
```

```
% Clear the matrix
dum=0;
K=subs(K);
FEM=subs(FEM);

%Assign constraints to the nodes
switch numMember
    case 5
        Ext=[V1;M1;V2;M2;V3;M3;V4;M4;V5;M5;V6;M6];
        fi=[d1;fi1;d2;fi2;d3;fi3;d4;fi4;d5;fi5;d6;fi6];
        M1=0;
        M2=0;
        M3=0;
        M4=0;
        M5=0;
        M6=0;
        d1=0;
        d2=0;
        d3=0;
        V4=0;
        d5=0;
        V6=0;
        unk=[fi1;fi2;fi3;fi4;fi5;fi6;V1;V2;V3;d4;V5;d6];
    case 6
        Ext=[V1;M1;V2;M2;V3;M3;V4;M4;V5;M5;V6;M6;V7;M7];
        fi=[d1;fi1;d2;fi2;d3;fi3;d4;fi4;d5;fi5;d6;fi6;d7;fi7];
        M1=0;
        M2=0;
        M3=0;
        M4=0;
        M5=0;
        M6=0;
        M7=0;
        d1=0;
        d2=0;
        d3=0;
        d4=0;
        V5=0;
        d6=0;
        V7=0;
        unk=[fi1;fi2;fi3;fi4;fi5;fi6;fi7;V1;V2;V3;V4;d5;V6;d7];
end

%Solve global stiffness equation
eqn=(Ext==K*fi+FEM);
solve(eqn);
sol=solve(eqn,unk);

%Assign results to each node
switch numMember
    case 5
     fi1=subs(sol.fi1);
     fi2=subs(sol.fi2);
```

```
     fi3=subs(sol.fi3);
     fi4=subs(sol.fi4);
     fi5=subs(sol.fi5);
     fi6=subs(sol.fi6);
     V1=subs(sol.V1);
     V2=subs(sol.V2);
     V3=subs(sol.V3);
     d4=subs(sol.d4);
     V5=subs(sol.V5);
     d6=subs(sol.d6);
    case 6
     fi1=subs(sol.fi1);
     fi2=subs(sol.fi2);
     fi3=subs(sol.fi3);
     fi4=subs(sol.fi4);
     fi5=subs(sol.fi5);
     fi6=subs(sol.fi6);
     fi7=subs(sol.fi7);
     V1=subs(sol.V1);
     V2=subs(sol.V2);
     V3=subs(sol.V3);
     V4=subs(sol.V4);
     d5=subs(sol.d5);
     V6=subs(sol.V6);
     d7=subs(sol.d7);
end

 %Solve element stiffness matrix equations
 for i=1:numMember
 element(i).deflection =fi(2*i-1:2*i+2);

element(i).forces=subs(element(i).stiffness*element(i).deflection+e
lement(i).FEM);
 end
```

c.createElement.m

```
function element=createElement(q,L,S,start,toe)
element(1).stiffness=[12*S/L^3 6*S/L^2 -12*S/L^3 6*S/L^2;
                      6*S/L^2 4*S/L -6*S/L^2 2*S/L;
                      -12*S/L^3 -6*S/L^2 12*S/L^3 -6*S/L^2;
                      6*S/L^2 2*S/L -6*S/L^2 4*S/L];
element(1).FEM=[q*L/2; q*L^2/12; q*L/2; -q*L^2/12];
element(1).coor=[start,toe];
end
```

B. SAP2000 Verification

SAP2000 models are prepared to verify the MATLAB code prepared for the initial stage analysis model with the 2 launched support. All support joints are modeled as pin joints, as mentioned in Chapter 4. The following configuration (Figure B.1) is used for the deck cross-section.

- Unit Weight=25 kN/m^3
- A=14 m^2
- I=22.75 m^4
- E=36 GPa
- L=60m

For the launching nose, below set of parameters is chosen:

- α_L=0.5 α_q =0.1 α_{EI} =0.2 – Normal launching nose

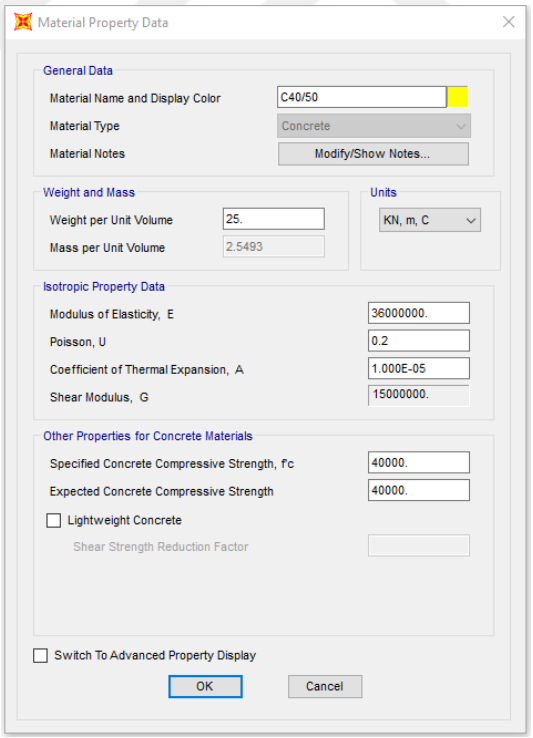

Figure B.1. The material property of the deck cross-section

Four different increment steps of the launching are chosen for the comparison. These increment steps cover both phase 1 and phase 2 of the launching (Table B.1).

Table B.1 Increment Steps

	Phase 1	End of Phase 1	Start of Phase 2	Phase 2
α	0.25	0.50	0.50	0.75
x	15m	30m	30m	45m

Figure B.2, B.3, B.4, and B.5 show the moment diagrams for different increment steps on SAP2000.

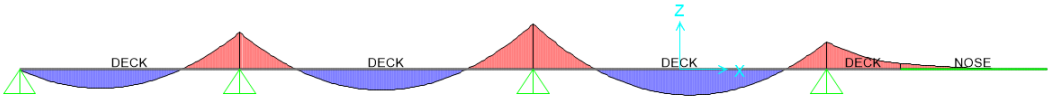

Figure B.2. Moment diagram for x=15m

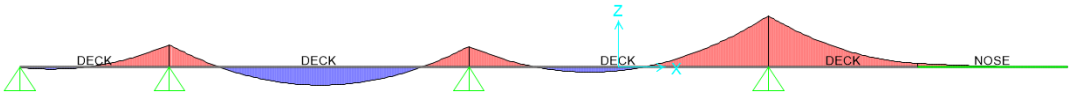

Figure B.3. Moment diagram for x=30m, just before nose touch support A

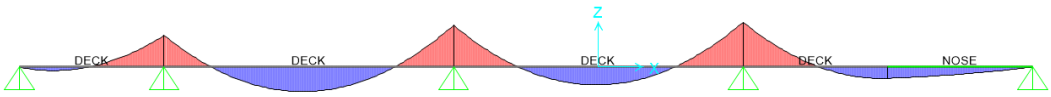

Figure B.4. Moment diagram for x=30m, nose reached support A

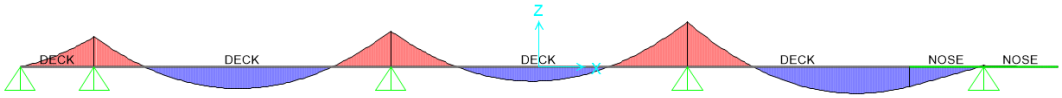

Figure B.5. Moment diagram for x=45m

Table A.2, A.3, A.4, and A.5 shows the differences between MATLAB structural analysis code and the SAP2000 results. Differences for all examined parameters are lower than the %0.1. Therefore, it can be said that the structural analysis code prepared on MATLAB is in agreement with the SAP2000.

Table A.2. Percent Differences for the x=15m

	R_B (kN)	M_B (kN-m)	M_C (kN-m)
SAP2000	16041	-70850	-116040
MATLAB	16042	-70812	-116090
Difference	0.01%	-0.05%	0.04%

Table A.3. Percent Differences for the x=30m, just before nose touch support A

	R_B (kN)	M_B (kN-m)	M_C (kN-m)
SAP2000	24058	-204678	-83732
MATLAB	24061	-204630	-83792
Difference	0.01%	-0.02%	0.07%

Table A.4. Percent Differences for the x=30m, nose reached support A

	R_B (kN)	M_B (kN-m)	M_C (kN-m)
SAP2000	20691	-115775	-107978
MATLAB	20698	-115820	-108020
Difference	0.03%	0.04%	0.04%

Table A.5. Percent Differences for the x=45m

	R_B (kN)	M_B (kN-m)	M_C (kN-m)
SAP2000	22907	-128901	-103598
MATLAB	22913	-128950	-103640
Difference	0.03%	0.04%	0.04%